Small Volcanic Vents of the Tharsis Volcanic Province, Mars

J. A. Richardson[1,2*], J. E. Bleacher[2], C. B. Connor[3], L. S. Glaze[4]

[1]Department of Astronomy, University of Maryland, College Park, MD, USA 20742
[2]Planetary Geology, Geophysics, and Geochemistry Laboratory, NASA Goddard Space Flight Center, Greenbelt, MD, USA 20771
[3]School of Geosciences, University of South Florida, Tampa, FL, USA 33620
[4]Planetary Science Division, Science Mission Directorate, NASA, Washington, DC, USA 20546

Key Points:

- We present a catalog of 1106 small volcanic vents identified within Tharsis Volcanic Province.
- Distributed-style volcanism has been common throughout Tharsis history and has been affected by large volcanoes and regional fossae.
- Recent (≤500 Ma) magmatism near the Tharsis Montes created volcanic fields to the east and rift apron lavas between the large shields.

*Current address, NASA Goddard Space Flight Center, MS 698, 8800 Greenbelt Road, Greenbelt, MD, USA 20771; ORCID ID: 0000-0002-1736-8907

Corresponding author: Jacob Richardson, `jacob.a.richardson@nasa.gov`

Abstract

Distributed-style volcanism is an end member of terrestrial volcanism that produces clusters of small volcanoes when isolated magma bodies ascend from broad magma source regions. Volcano clusters can develop over millions of years, one volcano at a time, and can be used to infer unobserved geologic phenomena, including subsurface stresses and cracks during eruption periods. The Tharsis Volcanic Province covers approximately one-quarter of the martian surface and hosts a large concentration of small volcanoes that formed from distributed volcanism. We present a catalog of 1106 small volcanic vents identified within Tharsis Volcanic Province. This catalog includes morphologic measurements for each cataloged vent. Vent lengths range from 71 m to 51 km, widths range from 40 m to 3.1 km, and 90% of vents have lengths at least 1.5 times their widths. Additionally, 90% of edifices associated with vents have topographic prominences <100 m. Vents are found throughout Tharsis, though they generally form clusters near large volcanoes or among large graben sets. Older regions with volcanic eruption ages of >1 Ga are found at the Tharsis periphery in the Tempe-Mareotis region and Syria Planum. Vents in the Tharsis interior have reported ages <500 Ma. Regional trends in vent orientation and intervent alignment are dependent on nearby central volcanoes and fossae. We use these findings to hypothesize that within the most recent 500 Ma, magma was present under and to the east of the Tharsis Montes and that some of this magma erupted and built hundreds of small volcanoes in this region.

Plain Language Summary

Clusters of small volcanoes are formed over long periods of time (hundreds of thousands of years to tens of millions of years). They form when magma is present underground but is not voluminous or concentrated enough to form a single magma chamber when it ascends that would otherwise create a large, central volcano. At Mars, a large region called the Tharsis Volcanic Province has both very large volcanoes and many small volcanoes. We have used images taken in orbit around Mars to map 1106 small volcanic vents. We used images and topography data to measure the sizes of volcanic vents. Most vents are significantly longer (up to 51 km) than they are narrow, while only 10% are circular. Most small volcanoes are short: less than 100 m tall. Vents are as young as a few million years, while some are over 3 billion years old. Their arrangement is also dependent on the neighboring large volcanoes and fractures. We use these findings to hypothesize that within the most recent 500 million years, magma was present under the three large volcanoes in Tharsis, the Tharsis Montes, and that this magma created hundreds of small volcanoes in the center of the study region.

1 Introduction

Distributed-style volcanism, where eruptions occur over a broad area and do not coalesce into a single central volcano, is observed on Venus, Earth, the Moon, and Mars (Head et al., 1992; Spudis et al., 2013; P. J. Mouginis-Mark et al., 1992) and is a significant end member of volcanism that occurs under conditions where subsurface magma generation is regional but processes which focus melt into major ascent pathways are limited (G. A. Valentine & Connor, 2015). Small volcanoes that form clusters on terrestrial surfaces are manifest products of this style of volcanism. On Mars, like Earth, distributed-style volcanism emplaces lava flows, cones, and low shields which are sometimes considered to be “monogenetic” (Kereszturi & Németh, 2013; Greeley, 1977; Hauber et al., 2009). While the surface of Mars has also preserved flood lavas (Jaeger et al., 2010), large shield volcanoes (Carr, 1973), regional ash deposits (Kerber et al., 2012), and large calderas (Michalski & Bleacher, 2013; Williams et al., 2009) that are each evidence of focused, large volumes of magma erupting over the surface, clusters of small volcanoes record the magmatic history of Mars during periods and regions where magma was otherwise unable to erupt to form massive central edifices.

Questions remain about how clusters of small volcanoes, or volcanic fields, form on Mars, especially in relation to large volcanoes. Is distributed volcanism primarily a product of waning volcanism at large volcanoes? Similar patterns exist on Hawaiian shield volcanoes Mauna Kea, Kohala, and Hualālai (Porter, 1972; Moore & Clague, 1992; Bleacher & Greeley, 2008; Rowland & Walker, 1990) and Galápagos Volcán Fernandina (Rowland, 1996) where waning magma supply has halted or limited main flank development, giving way to distributed volcanism and the formation of parasitic cones. However, some volcanic fields on Mars appear to be distant from large volcanoes (e.g. Tempe-Mareotis, Syria Planum) and might be formed from magma production events unrelated to those that supplied the larger volcanoes. Additionally, what is the spatial distribution of distributed-style volcanism? When was distributed-style volcanism active and how long-lived is this style of volcanic activity on Mars? Answering these questions can better constrain our understanding of the magmatic history of Tharsis as well as how the martian atmosphere was sustained in the geologic past (Halevy & Head III, 2014) and how frequently regions of the subsurface might be heated to sustain liquid water aquifers (Sori & Bramson, 2019).

The Tharsis Volcanic Province on Mars hosts not only the largest volcanic edifices in the Solar System (Carr, 1974), but also a large concentration of small volcanoes that formed from distributed volcanism (Hauber et al., 2009; Richardson et al., 2018). The varied volcanic products in the region suggests that Tharsis has been built by a number of magmatic production events of varying duration and magnitude from the late Noachian to the near present (Tanaka et al., 2014). Small volcanoes that have been dated in this region include the oldest volcanic products in Tharsis, dating to the early Hesperian Period (Richardson et al., 2013; Tanaka & Davis, 1988) and the youngest, with some features' ages being just 10s Ma (Hauber et al., 2011; Richardson et al., 2017).

In this paper, we investigate the occurrence and patterns of distributed volcanism within the Tharsis Volcanic Province. The primary features created from distributed volcanism are volcanic vents—where magma erupts at the surface of a planet to expel lava and/or tephra. Here we present a catalog of over 1000 small ($\leq$ 10 km) volcanic vents in the Tharsis Volcanic Province and we use this catalog to identify spatial and temporal trends in distributed-style volcanism in Tharsis. Distributed-style volcanism is an important element in the thermal evolution of terrestrial planets; while individual eruptions are not always as voluminous as those at central volcanoes, the creation of an entire cluster of dozens to hundreds of small volcanoes can deliver the same amount of magma to the surface as a central volcano over a longer period of time.

1.1 The Tharsis Volcanic Province

We consider the entire Tharsis rise our study area, which is loosely bounded by the hemispheric dichotomy boundary (D. E. Smith & Zuber, 1996) to the north and west, Echus Chasma to the east, and Thaumasia and Terra Sirenum to the south (Figure 1). Virtually all of the region that can be considered the Tharsis rise lies at elevations above the martian mean datum elevation, though the search for small volcanic vents also extends into the low trough west of Olympus Mons, which is below mean datum. This study area roughly centers on Ascraeus Mons, has a radius of over 2,000 km, and has an area of 13.6 million km^2, one-quarter of the Martian surface.

Regional Tharsis geology has been mapped as part of a global geologic map by Tanaka et al. (2014), who identified the bulk of the province's surface as Amazonian and Hesperian units of lobate lava flows primarily sourced from the Tharsis Montes. The Tharsis Montes are a line of three large shield volcanoes including Ascraeus Mons, Pavonis Mons, and Arsia Mons, whose surfaces are interpreted to be Amazonian in age as well. On the west of and superposing these large shield volcanoes are concentric, ribbed units that are interpreted to be drop moraines of alpine glacial systems (Scanlon et al., 2015). The vast volcanic flow unit covering most of the Tharsis Rise ("AHv", Tanaka et al., 2014) embays plateaus of older Hesperian volcanic units that are cut by sets of graben and abuts older Hesperian and Noachian aged highland units. Flows in this unit also contain the rift apron flows of the Tharsis Montes, which are scallop shaped rises abutting the north and south flanks of each large shield of the Tharsis Montes (Bleacher, Greeley, Williams, Cave, & Neukum, 2007; Crumpler & Aubele, 1978). Flows that make up these aprons are hundreds of millions years of age compared to the main Tharsis Montes flanks that have surface ages of >1 Ga from crater retention rate modeling (Werner, 2009). Olympus Mons and Alba Mons are also within the study area along its northwestern periphery.

Within the boundaries of Tharsis lie several previously described terrains with clusters of small volcanic vents, including the Tempe-Mareotis region (Tanaka et al., 2014), parasitic vents on the Tharsis Montes (Bleacher et al., 2009) and near Olympus Mons (Bleacher, Greeley, Williams, Werner, et al., 2007; Peters & Christensen, 2017), and Syria Planum (Richardson et al., 2013). Many of these terrains are denoted as volcanic field units in work by Tanaka et al. (2014). Additionally, large sets of parallel and curvilinear graben cut much of the terrain and have been previously interpreted to be the surface expression of shallow subsurface dikes, the vast majority of which do not intersect the surface and create volcanic vents (Mège & Masson, 1996).

2 Methods

In order to understand the history of distributed volcanism throughout the Tharsis province, we 1) catalog observed vents based on image and topography data; 2) perform a cluster analysis on the vent catalog to divide the Tharsis vent catalog into discrete regions to analyze individually; 3) measure vent and volcanic edifice characteristics to evaluate morphologic trends; and 4) identify intervent alignment orientations between nearby volcanic vents.

2.1 Mapping

2.1.0.1 Vent identification To identify and characterize each volcanic vent presently exposed at the martian surface, we assemble a catalog of vents observed in image and topography datasets over the entire Tharsis study area (Figure 1). We define the morphology of a volcanic vent in Tharsis to be a topographic depression where constructional lava flow features or pyroclasts extend from the depression. Vents are tens of meters to a few kilometers in length or diameter and their surrounding volcanic constructs are generally one to tens of kilometers in diameter with slopes of 0.5-4° and heights of 10-1,000 m (Hauber et al., 2009). Each identified vent is initially cataloged as a geographic point location that is situated at the center of the vent.

Volcanic vents are commonly situated at the summit of a larger topographic feature, specifically low shields or pyroclastic cones, which might be circular or elongate parallel to the vent depression. Some low shields with quaquaversal lava flows and knobs that are similar in size and slope to other pyroclastic cones in the region do not exhibit intact volcanic vents. This might be because of erosion of the vent, burial by dust, or because the final vent structure was buried by final lava flows or spatter at the volcano summit. To include these features in the catalog but separate them as distinct from identified vents, the summits of these interpreted volcanoes are defined as "likely vents," following the interpretation by Richardson et al. (2013). As with the visible cataloged vents, these likely vents are cataloged as a geographic point location situated at the apex of the volcano.

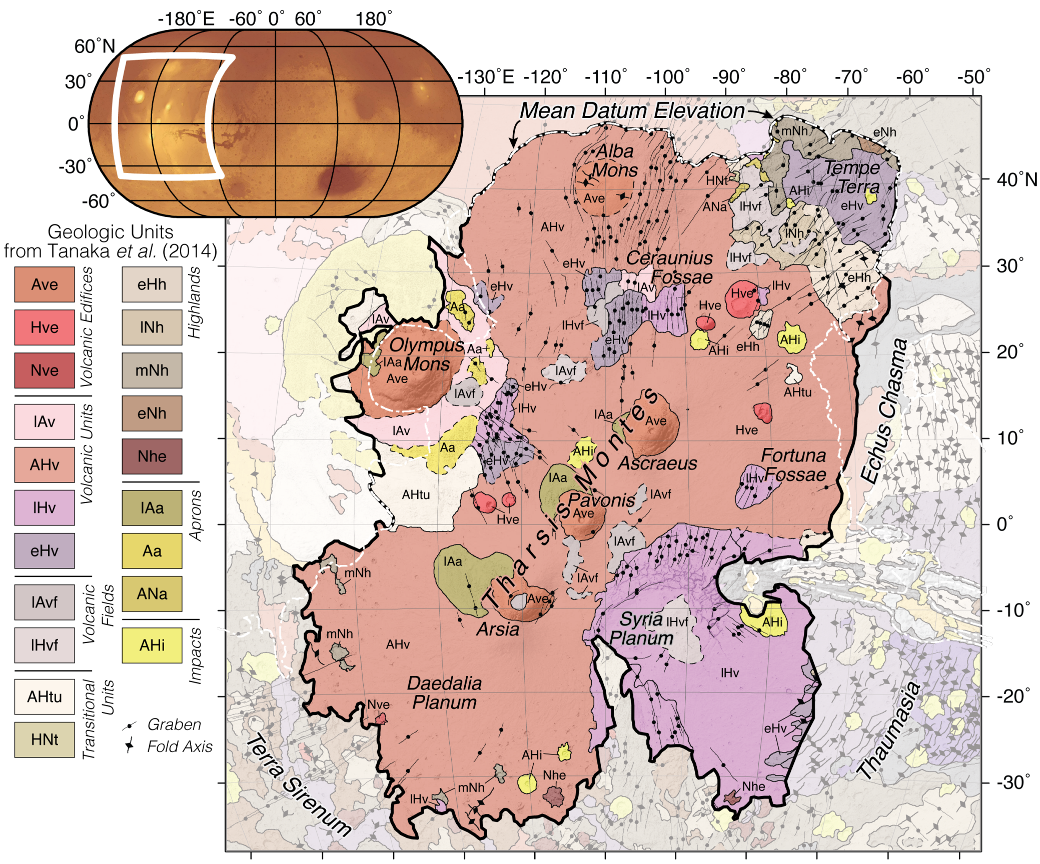

Figure 1. Geologic map of the Tharsis Volcanic Province (units from Tanaka et al. (2014)). The study area is outlined in solid black and encompasses the main volcanic edifices and units of Tharsis, which were active from the late Noachian to the late Amazonian epoch. See Tanaka et al. (2014) for unit descriptions. The mean elevation of Mars is annotated as a white dashed line and defines the northern boundary of the study area.

Many existing pits or depressions in Tharsis have similar morphologies to cataloged vents but without eminating flow features and surrounding topographic rises it is unclear that they were the site where magma erupted at the surface or if their provenance is tectonic or impact related. Such features with no evidence of volcanic deposits are not cataloged.

The catalog was produced in ArcGIS (versions 9.3-10.2) using the Mars 2000 datum as a coordinate system and all geographic locations in the catalog are recorded in decimal degree format. We used the 512 pixels-per-degree (ppd) Thermal Emission Imaging System (THEMIS) infrared daytime mosaic (Christensen et al., 2004) and the 128 ppd Mars Orbiter Laser Altimeter (MOLA) (D. Smith et al., 2003) gridded data set as co-referenced basemaps. To identify vents that are at the limit of recognition using the basemaps alone, higher resolution, georeferenced images from High Resolution Stereo Camera (HRSC) (Neukum et al., 2004), Context Imager (CTX) (Malin et al., 2007), and THEMIS Visible data sets were used. Images from the CTX and THEMIS now each provide virtually complete coverage of the study area with spatial resolutions of 6 m- and 19 m-per-pixel respectively, enabling the cataloging effort to identify the smallest of volcanic vents. To ensure completeness of the catalog, the entire study area (Figure 1) was systematically surveyed with these high-resolution image data sets for all features matching the morphological definition for a volcanic vent or likely volcanic vent. The resulting catalog is a minimum estimate of the number of distributed-style volcanic vents that have formed within Tharsis as many have likely been buried by more recent flows or aeolian deposits, destroyed by faulting or erosion, or remain undetected in this study due to ambiguous morphology.

2.1.0.2 Cluster analysis In order to identify spatial trends in the vent catalog over the entire study area, regions of vents within Tharsis are identified and the morphologies and arrangements of the vents within these regions are compared. These regions within Tharsis are defined using the vent catalog itself through a hierarchical clustering algorithm.

The hierarchical clustering analysis is performed using all vent locations, including likely vents, in the Tharsis catalog. This approach is agglomerative (*i.e.*, bottom up) and follows the Unweighted Pair Group Method with Arithmetic Mean approach, where individual vents are added to nearby clusters depending on their distance to the centroid of that cluster. All distances are measured along great-circle paths assuming a Mars spheroid of radius 3390 km. The analysis results in a hierarchy of clusters of vents that can be illustrated as a dendrogram, with clusters separated from others by the distances between their respective centroids.

Regions in the Tharsis vent catalog are identified in this analysis as clusters of vents where all vent locations lay within 600 km of the cluster centroid. This distance is the approximate width of Olympus Mons and the volcanic fields in Syria Planum and Tempe Mareotis (Figure 1), which might be a reasonable choice if the regional extent of a typical magma generation event was about this size, but this distance is chosen simply to identify regional trends of the vents with no interpretation that the resulting regions of vents are isolated volcanic fields.

2.2 Vent and edifice morphology

2.2.0.1 Vent Dimensions The length and width of each volcanic vent in this dataset are measured. The length of the vent is its longest dimension and the width of the vent is the distance across the depression perpendicular to and at the midpoint of the trace of the vent length. While some vents are large enough to measure with the THEMIS basemap, most of these measurements were taken using georeferenced CTX images. Each vent is assigned two vent endpoint coordinates (latitude, longitude), which correspond to the two ends of the longest dimension, along with the vent length (meters) and vent width

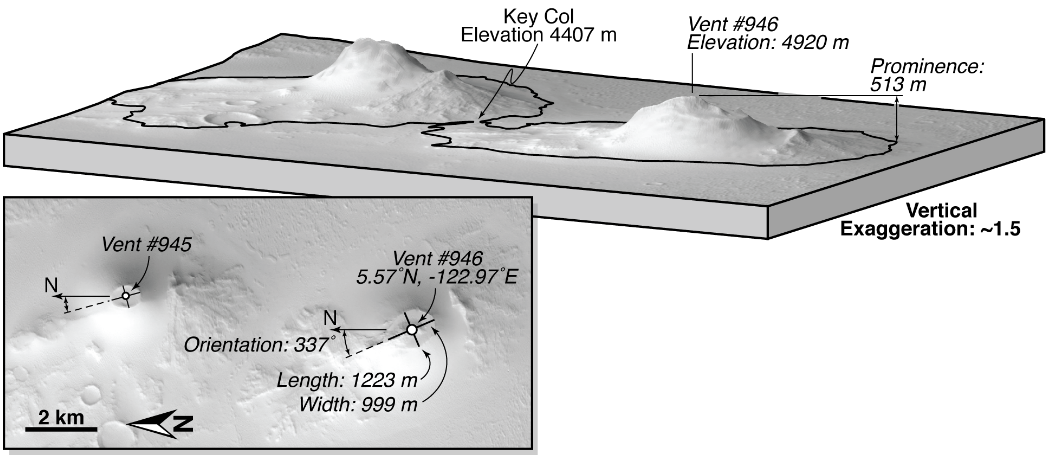

Figure 2. Vent lengths, widths, and orientations to North are measured for all vents. Prominence is measured as a proxy of height as the difference between summit elevation and an automatically identified *key col* elevation. These example vents are located within Ulysses Fossae and are illustrated with a perspective view created with CTX images (F18_042652_1855_XN_05N123W and P19_008262_1862_XN_06N123W) within Ames Stereo Pipeline (Beyer et al., 2018).

(meters). Vent lengths are automatically calculated using the great-circle distance between their two endpoints, while vent widths, which are generally $<$1 km, are measured manually in ArcGIS. These measurements are not made for cataloged likely vents which do not exhibit a depression.

2.2.0.2 Prominence Other morphologic measurements of volcanoes (*e.g.*, height, area, average slope) require mapping the areal extent of the edifice or associated deposits. This mapping has been performed in the Tharsis region before (e.g., Baptista et al., 2008; Richardson et al., 2017), but such mapping is inhibited at many locations in Tharsis due to dust cover and embayment by younger lava flows. Instead of attempting to perform this mapping at each vent in the catalog and defining a topographic base to make height measurements with, we measure the topographic prominence of each vent and likely vent in the catalog.

Topographic prominence is the vertical relief between a peak and its *key col*, which is the lowest surrounding closed contour line within which the peak lays at the highest elevation. As an example, Pavonis Mons (peak elevation, 14 km above the mean datum) has a prominence of 6.6 km as its *key col* is at 7.4 km elevation. Contours enclosing Pavonis Mons below 7.4 km above mean datum also enclose the higher summit at Arsia Mons (peak elevation 17.6 km). Arsia can be considered to be the parent peak of Pavonis Mons. By comparison, Arsia Mons has a prominence of 12.1 km with Ascraeus Mons as its parent peak. Alternate methods to defining volcano height are possible and require the observation of either lava flow fronts or breaks in slope to define a volcanoes boundary. We elect to use prominence because lava flow fronts are often buried by dust or more recent lava flows on Tharsis and tools to identify slope breaks (e.g., Bohnenstiehl et al., 2012) require a number of *a priori* selection parameters that might not be appropriate for the entire vent catalog. Following a slope break method, Arsia's height can be described as 10.6-11.9 km by defining its base as breaks in slope to the volcano's southeast and northwest, similar to its topographic prominence value of 12.1 km.

Prominence for every vent is measured using the peak elevation of the volcanic edifice it created, which is defined here as the highest point immediately adjacent to the vent depression, according to the gridded MOLA topographic dataset. The summit elevations of likely vents are also used to calculate topographic prominence.

Some volcanic landforms might also not have a measureable topographic prominence if they are emplaced on the flanks of a large slope including the flank of a larger volcano or if they are very low profile. For the former case, even though the vent erupted a topographically positive landform, the landform is a morphologic "shoulder" on the slope and does not have a single enclosing contour. For all vents and likely vents whose surrounding deposits do not have a single enclosing contour at 1 m vertical resolution, a topographic prominence of $\leq$1 m is assigned, as these vents' edifices either have no prominence or a prominence below the vertical resolution of the MOLA dataset. The MOLA Gridded dataset has a vertical resolution of 1 m (Som et al., 2008) and is used because of its global coverage. While elevation values in the dataset are interpolated between laser ranged points of the martian surface, Som et al. (2008) found that 96% of locations have a real laser shot within 3.7 km, which is smaller than the diameter of most of the features in this catalog.

2.3 Vent arrangement

2.3.0.1 Vent orientation Orientation is measured for each volcanic vent using the vent endpoints recorded in the vent dimensions analysis above. Orientation is measured as the bearing of the major axis of the vent with respect to north. A categorical exception to this method is vents that are not elongate, where major axis length is less than 1.5 times the minor axis length; these vents are assigned no orientation but are labeled as "equant." Cataloged likely vents that do not exhibit a depression are excluded from this measurement.

Vent orientations are compared to vent direction from the four large volcanoes: Olympus Mons, 18.3°N, 133.2°W; Ascraeus Mons, 11.2°N, 104.4°W; Pavonis Mons, 0.8°N, 112.5°W; and Arsia Mons, 9.2°S, 120.4°W. Given the lack of cataloged vents near Alba, vent orientations are not compared to direction from the Alba Mons summit. If a volcanic vent is co-oriented with its direction from a large volcano, it is considered to be radially oriented. If the volcanic vent orientation is perpendicular to its direction from a large volcano, it is considered to be circumferentially oriented. Vent-volcano alignment is measured as being between 0-90°, with 0 being perfectly radial and 90 being perfectly circumferential without respect to the sense of alignment (e.g., clockwise or counterclockwise). While a vent aligned at $< 45°$ is technically more radial than circumferential, we adopt alignment angles $< 30°$ to be generally radial and alignments $> 60°$ to be generally circumferential.

For this analysis, central volcano locations are defined as the coordinates at the center of their summit caldera complexes, to the nearest tenth of a degree ($\sim$6 km) to account for uncertainty of the location of each volcano's center. For a vent 100 km from the summit, this results in an vent-volcano alignment uncertainty of about 3.5°.

2.3.0.2 Vent alignments Predominant orientations of intervent alignments have been previously observed for clusters of volcanoes on Mars and Earth to identify preferred orientations of igneous pathways, such as dikes, in the subsurface (Wadge & Cross, 1989; Richardson et al., 2013; Christoph & Garry, 2017). We determine significant intervent alignments between vents within each region identified in the cluster analysis using a two-point azimuth method (Wadge & Cross, 1988; Cebriá et al., 2011). The two-point azimuth method measures the orientations of all line segments that connect all vent locations to other vent locations. Significant intervent alignments are then considered to be orientations that are most common. To identify these modal orientations, orientations are grouped in swaths of 20°. One modification to this method was made by Cebriá et

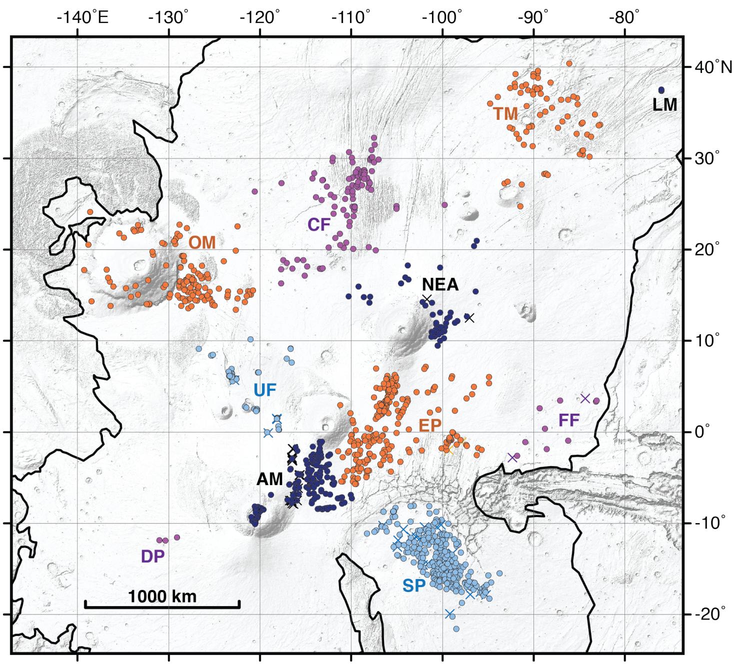

Figure 3. Cataloged small vents within Tharsis. Vent color corresponds to regions identified using cluster analysis of the entire catalog: OM, Olympus; CF, Ceraunius; UF, Ulysses; DP, Daedalia Planum; TM, Tempe-Mareotis; NEA, Northeast Ascraeus; EP, East Pavonis; AM, Arsia; SP, Syria Planum; FF, Fortuna; LM, Labeatis Mons. Circle symbols are mapped vent features, crosses are mapped likely vents. The solid outline is the study area boundary and a shaded relief map is used as a basemap. No vents are cataloged within the study area beyond the extent of this map.

al. (2011), where only relatively short distance line segments—connecting vents that are relatively nearby each other—are considered. This is because long distance line segments, which connect distant vents, will be oriented along the major axis direction of the volcano cluster itself and are therefore more useful indicators of overall cluster shape than they are of related vents. An added advantage of the Cebriá method is that nearby vents are more likely to have related crustal ascent pathways than distant vents, and preferred alignments between vents are therefore more easily recognized. Cebriá et al. (2011) decided to use two-point azimuths that are smaller than one-third the mean length of all intervent line segments. This same criteria is applied to intervent connections in each region identified in the cluster analysis above.

3 Results

3.1 Mapping

3.1.0.1 Vent identification Within the Tharsis Volcanic Province, we identify 1106 small volcanic vents or likely vents (Figure 3, Supplemental Table 1). Of the cataloged features, 1047 are interpreted to be volcanic vents given their observable topographic depressions with flow features extending from them (Figure 4*a*-*h*). The other 59 likely vent features in the catalog are assumed to be vent locations where magma erupted at the surface, due to the presence of a low shield volcano or likely pyroclastic cone, but do not have observable depressions (Figure 4*i*).

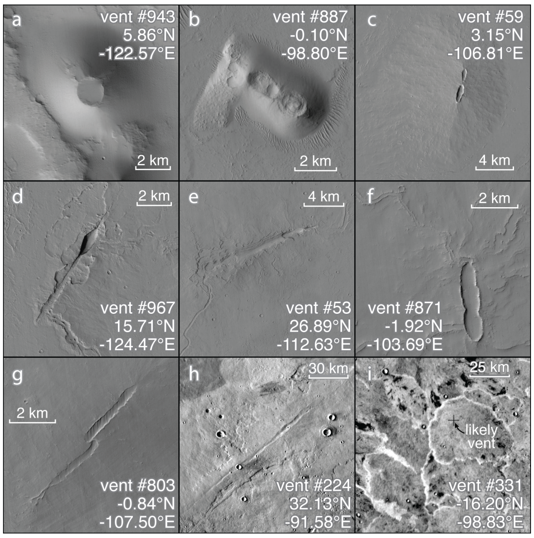

Figure 4. Example vents identified in the study area. a,b) Pyroclastic cones. c) a low shield. d-f) elongate vents often have channels extending downslope from their ends. g) an *en echelon* vent. h) This 50-km long fissure vent build a linear edifice about 15 m high. i) Coalesced vents in Syria Planum. The central edifice has no physiographic vent depression at its summit, though the surrounding similar features do and its summit is labeled as a "likely vent." Image sources a-g: CTX; h,i: THEMIS.

The cataloged vents are found throughout the Tharsis Province of Mars, between 21°S–40°N, 76°W–139°W. Small vents are found at virtually all elevations of Tharsis, from the trough of Olympus Mons, 2.4 km below mean datum to 16.5 km above mean datum at the summit of Arsia Mons. The majority of vents lie between 0-10 km elevation.

Concentrations of vents can be seen in several places, including at the eastern base of Olympus Mons, to the east of the Tharsis Montes, within Syria Planum, and amongst the Ceraunius Fossae and the Tempe and Mareotis fossae. Several regions are also devoid or nearly devoid of vent features, including Alba Mons, Daedalia Planum, regions surrounding Tharsis Tholus, Noctis Labyrinthus, and the flanks and summits of the large volcanoes, except the flanks of Olympus Mons and the Arsia Mons summit. It is unclear if these regions have always been devoid of volcanic source vents or if burial has erased them from the current surface.

3.1.0.2 Cluster analysis Through hierarchical cluster analysis, the 1106 features in the vent catalog are separated into 11 regions. All vents within each region are less than 600 km from the region's geographic centroid, calculated as the mean latitude and longitude of all the region's vents. Vent population size within each region varies dramatically from 267 in Syria Planum to regions around the boundaries of the study area that contain just three (Labeatis Mons and Daedalia Planum) vent features. Summary statistics for each defined region are listed in Table 1.

Some regions comprise volcanic vents that are more isolated that the rest of the catalog, including Syria Planum and Tempe Mareotis. In other identified regions, vents are closely spaced to vents in adjacent regions, especially between the Arsia and East Pavonis regions. Because of this, we do not interpret each identified region to necessarily be a geologically separate volcanic field of vents. Instead, these regions are used below to describe trends in the vent catalog across Tharsis.

Table 1. Regions of vents in Tharsis

	Count			Centroid	
Name	Total Vents	Equant Vents	"Likely" Vents	Latitude	Longitude
Olympus	133	11	0	16.83°N	-128.34°E
Ceraunius	99	8	0	25.59°	-110.37°
Ulysses	51	15	4	4.86°	-121.12°
Daedalia Planum	3	0	0	-11.77°	-130.13°
Tempe-Mareotis	67	6	0	34.52°	-88.74°
Northeast Ascraeus	47	4	2	13.10°	-101.19°
Arsia	192	16	21	-5.77°	-115.33°
East Pavonis	231	18	2	0.83°	-105.50°
Syria Planum	267	30	28	-13.82°	-100.45°
Fortuna	11	2	2	0.69°	-87.75°
Labeatis Mons	3	2	0	37.46°	-75.97°

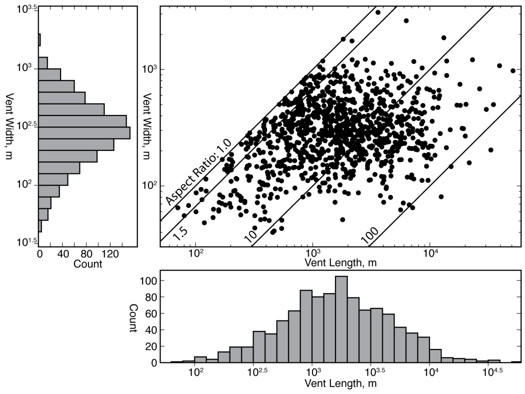

Figure 5. Histograms of vent length (bottom) and width (left) in Tharsis. Each vent is plotted as a circle in the top-right scatter plot, and annotated solid lines denote different aspect ratios from equant (1.0-1.5) to very elongate (100).

3.2 Vent and edifice morphology

3.2.0.1 Vent Length All vent features with clear depressions (*i.e.*, not features cataloged as "likely vents") are measured and lengths range from 0.071-51 km (Figure 5). Vent widths range from 0.040-3.1 km. Of note, while vent length varies by three orders of magnitude, vent width is more tightly bound, varying by only two orders. Aspect ratios of individual vents range from equant, 1.0, to very elongate at 160. Median aspect ratio is 5.2 and 90% of all vents have aspect ratios <24. We observe 935 of 1047 vents to be elongate, while 112 are equant with lengths $\leq 150\%$ vent width.

3.2.0.2 Prominence Using all vent and likely vent locations, 767, or 69% of vents have a topographic prominence greater than 1 m. Prominence of these features ranges from 2 m (the minimum measurable value) to 1.1 km; 90% of edifices surrounding vents are <100 m high, with a median prominence of 10 m. This range of prominence well describes all areas of Tharsis and all of the 11 vent regions have median prominence values ≤ 51 m (Figure 6).

The tallest volcanoes in this catalog are limited to a few regions of Tharsis; the regions East Pavonis, Syria Planum, Ulysses, and Fortuna each have edifices constructed

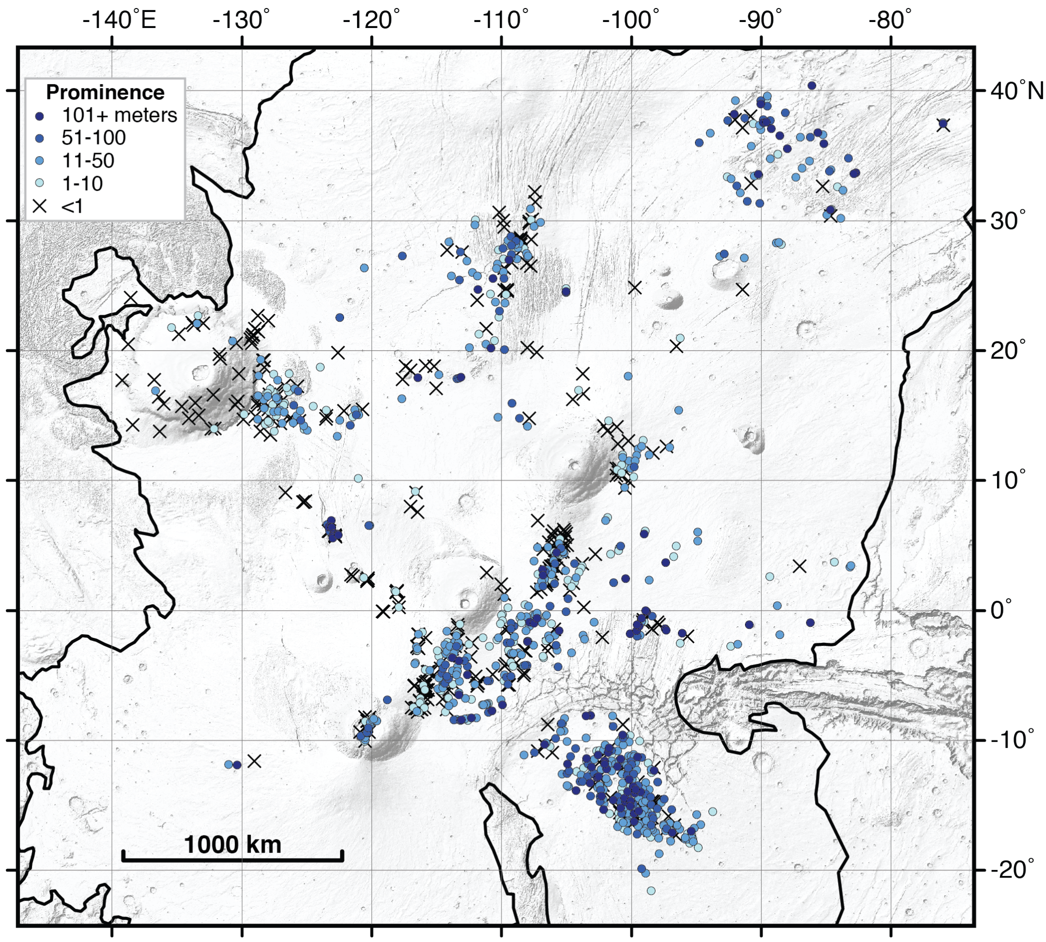

Figure 6. The Tharsis vent catalog shaded by prominence. Darkest circles are >100 m tall. X symbols represent vents with no measurable prominence. The most prominent vent is in Syria Planum.

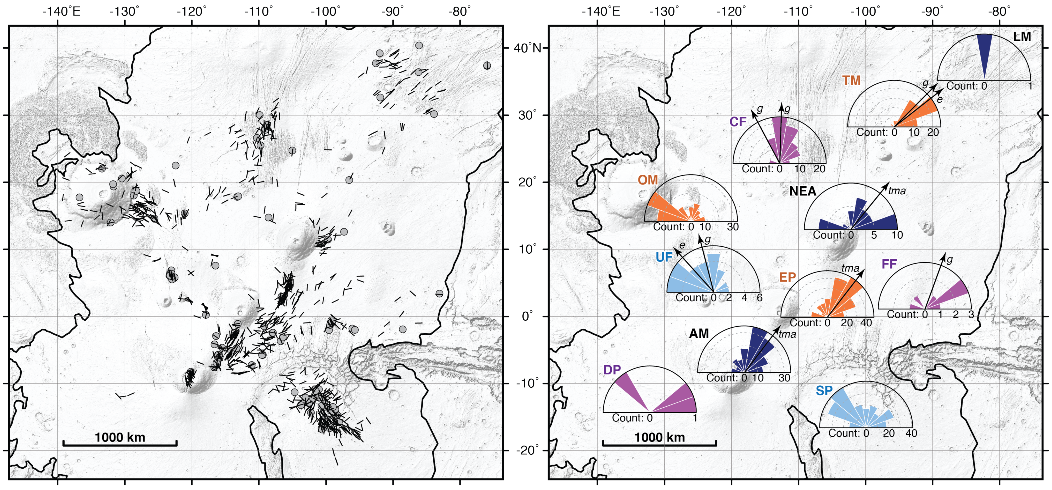

Figure 7. (left) Vent orientations mapped as oriented lines (symbols are all equal length and weight). Equant vents are mapped as gray circles. (right) Rose diagrams of vent orientation by vent region. In regions where features are aligned or indicate previous strain of the terrain, arrows superpose the rose diagrams. Arrow annotations include *g* (graben) and *tma* (Tharsis Montes Axis) and these arrows are co-aligned with these features. Additional arrows annotated *e* are oriented perpendicular to the direction of previously observed extensional strain. Region acronyms and colors are the same as Figure 3.

by small vents that are higher than 300 m. Most edifices that are >300 m high appear to have smooth surfaces, high slopes (5-20°) and diameters of 1-4 km (Figure 4*a,b*), consistent with the morphology of martian pyroclastic cones (Brož & Hauber, 2012). The most prominent feature (1.1 km) in the catalog, however, is a broad shield at the summit of a large ridge constructed by small vents in Syria Planum (Richardson et al., 2010).

Volcanic edifices with no measurable prominence are found in all regions. On the main flanks of Olympus Mons, 20 of the 26 identified vents do not have a measurable prominence. These edifices still are constructional landforms, but exist as shoulders on the regional slope instead of local topographic maxima. As the slopes of Olympus Mons at the elevations of the cataloged vents are around 4-6°, these 26 edifices might have considerable "height" if measured by alternate means. Other vents with low or no topographic prominence appear to be common in regions, far from large central volcanoes, where large graben sets are found and are often elongate fissure vents (*e.g.*, Figure 4*h*).

3.3 Vent arrangement

3.3.0.1 Vent orientation In each region across Tharsis, modal vent orientations of all directions are found, though clear modes of vent orientation appear to transcend individual regions (Figure 7b). The most prominent trend in vent orientation runs northeast, parallel to the axis of the Tharsis Montes, and extends from the Arsia region to the northeastern extent of the Tharsis rise in Tempe-Mareotis, where the trend curves to become slightly more east-oriented, parallel to the major graben features in the area. The bearings between neighboring peaks of the Tharsis Montes are plotted over vent orientation rose diagrams for the Arsia, East Pavonis, and Northeast Ascreaus vent regions as arrows in Figure 7b. At Arsia Mons, this axis bearing is N37.4°E; at Pavonis Mons the bearing is N37.7°E, and at Ascraeus Mons the bearing is N39.1°E. Orientations within the Arsia and East Pavonis regions are aligned with this axis, with mean orientations bearing N32°E and N36°E, respectively. Orientations within the Northeast Ascraeus region are not in line with this NE trend. Within the Tempe-Mareotis region, N45°E striking grabens have been mapped by Hauber and Kronberg (2001) and crustal extension along these fractures has been modelled by Golombek et al. (1996) to be oriented N38°W. Arrows over the Tempe-Mareotis rose plot in Figure 7b show these directions with one (annotated "g") is along the strike of the graben and the other (annotated "e") is plotted orthogonal to the direction of extension (i.e., N52°E), which would ideally be parallel to a dike that intruded during such extension. Here vent orientations are aligned with both grabens and extensional patterns with the majority of vent orientations bearing within 17° of either bearing.

Similar to Tempe-Mareotis, the plurality of vents in the Ceraunius region are oriented parallel to their eponymous fossae features. Most faults adjacent to the volcanic field in this region trend approximately N3°E, while western faults are curvilinear, trending N28°W. Vent orientations align with the north striking grabens, with the majority falling within 20° of N3°E. Vents in the Fortuna and Ulysses regions are less well aligned with regional fracture patterns. Fortuna Fossae faults strike approximately N20°E, while fossae in Ulysses, mapped by Fernández and Ramírez-Caballero (2019), have variable strikes but average N15°W. Extension in this region was also measured to have been N42°E (Fernández & Ramírez-Caballero, 2019), which would ideally lead to dike orientations of N48°W. In both regions, modal vent orientation is not aligned with any of these directions, though we note that both regions have small population sizes and a main cluster of vents in the Ulysses region (Brož & Hauber, 2012) have equant vent shapes.

Modal vent orientations in the Olympus and Syria Planum regions are to the northwest. In the case of Syria Planum, vent orientation is aligned with tectonic structures in Noctis Labyrinthus and are potentially radial to an early Hesperian tectonic center between Noctis Labyrinthus and Pavonis Mons identified by Anderson et al. (2001). In the case of the Olympus Region, these vents appear to be primarily oriented towards Olympus Mons itself.

Vents' orientations from each large volcano (Olympus, Ascraeus, Pavonis, and Arsia) are plotted as histograms from 0-90°, where 0 is radial and 90 is circumferential. The distribution of vent orientation is also filtered by distance from the volcano, with vents $\leq$500 km from the summit of a major volcano making up a "nearby" category, a "distant" category of vents >1000 km from the summit, and vents in between creating an "intermediate" category (Figure 8). Olympus Mons has a majority of nearby vents that are oriented within 30° of radial (57 of 103 vents), as does Ascraeus Mons (69 of 110 vents), and Arsia Mons (53 of 105 vents). Nearby vents at Pavonis Mons are, however, offset from radial or circumferential. With increasing distance, all central volcanoes except Pavonis have decreasingly radial relationships to small vents; the majority of distant vents to Pavonis Mons are radially oriented (249 of 431 vents). A plurality, 42% of vents, at large distances from Olympus Mons are circumferentially oriented to its summit. This trend and other orientations at large distances can be explained by vent orientation being governed by closer features than each central volcano. In the case of Olympus Mons, NE-oriented vents adjacent to the Tharsis Montes are within this most distant category.

3.3.0.2 Intervent alignments The two-point azimuth method of identifying local relationships between features is carried out for vent regions with at least 10 cataloged vents. This minimum vent count enables the identification of short intervent relationships that are not affected by the shape of the overall region. With this threshold, the analysis was performed on 9 of 11 vent regions (Figure 9).

Predominant intervent alignments in different regions are sometimes co-aligned with vent orientation, while in other regions modal vent orientation is not a predominant intervent alignment direction. Predominant intervent alignments along the Tharsis Montes are approximately parallel to the axis of the montes in the East Pavonis Region, sim-

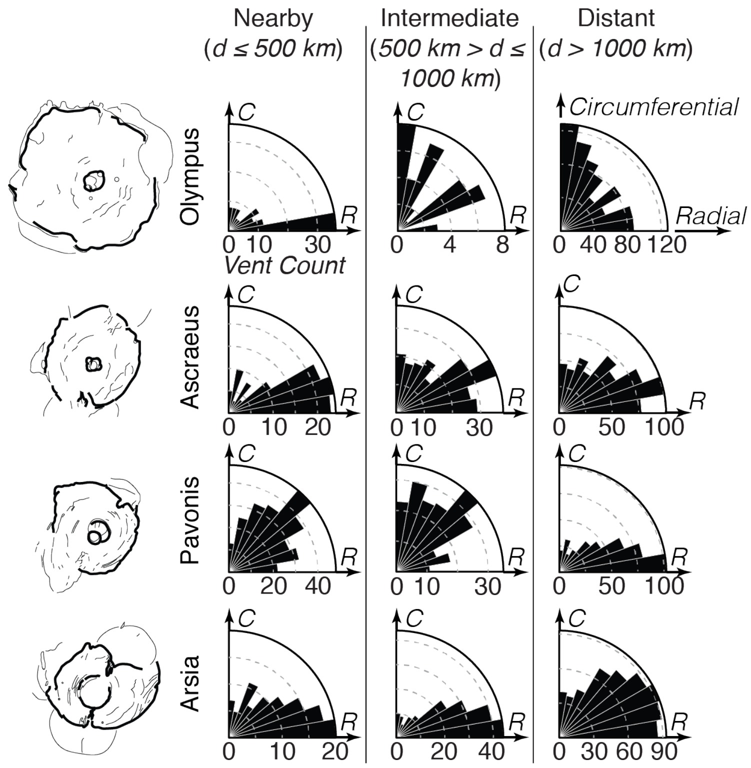

Figure 8. Orientation of vents with respect to the four central volcanoes of Tharsis, Olympus Mons, Ascraeus Mons, Pavonis Mons, and Arsia Mons, each sketched on the left. For each volcano, all vents in the catalog are binned by distance from the summit (nearby, intermediate, or distant). Rose diagrams illustrate the difference in degrees between vent orientation and the bearing from each vent towards each central volcano. Radial vents have major-axes that point toward central volcano summits, while circumferential vents' major-axes are perpendicular to the direction of a central volcano summit. Rose diagram petals have 10° widths.

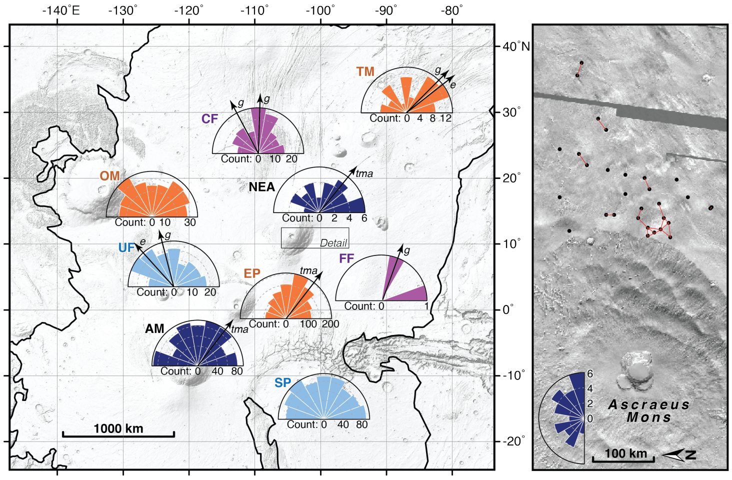

Figure 9. (left) Rose diagrams of local intervent alignments at the nine regions with more than ten vents. Like Figure 7, in regions where features are aligned or indicate previous strain of the terrain, arrows superpose the rose diagrams. Arrow annotations include *g* (graben) and *tma* (Tharsis Montes Axis) and these arrows are co-aligned with these features. Additional arrows annotationed *e* are oriented perpendicular to the direction of previously observed extensional strain. Region acronyms and colors are the same as Figure 3. (right) Detail of intervent relationships on the eastern flank of Ascraeus Mons. Vents are circles and the closest intervent distances are illustrated as red line segments. These relationships are potential vent alignments and they are predominantly oriented E-NE in this region.

ilar to modal vent orientations in this region, though this trend is not observed closer to Arsia or Ascraeus Mons. Within East Pavonis, the mean orientation of intervent alignments is N22°E, compared to the bearing from Pavonis Mons to its neighboring large shields of N38°E. The majority of alignments in this region are within 37° of parallel to this Tharsis Montes bearing.

In the Tempe-Mareotis Region, this northeast alignment direction is the largest modal alignment, with 34% of alignments lying between N30°E and N70°E. In this region, these alignments agree with extensional strain (Golombek et al., 1996) and graben (Hauber & Kronberg, 2001) directions which also fall within this orientation range. Similar to Tempe-Mareotis, in the Ceraunius region, vent alignments have a northward mean orientation of N8°E, parallel to vent orientation and the surrounding fossae. Here, the majority of alignments are within 40° of the north-striking grabens in the fossae. In the Ulysses region, alignments are not obviously oriented with the fossae but instead have a northwest modal direction towards Olympus Mons, with a mean bearing of N42°W. This preferred orientation is perpendicular to extensional strain measured by Fernández and Ramírez-Caballero (2019) and the majority of alignments are again within 40° of perpendicular to the direction of extension. Vent alignments at Syria Planum and Olympus Mons are less clearly modal.

4 Discussion

Vents in this study are interpreted to have formed as individual eruptions and the distributed construction of several to hundreds of vents over a region forms a volcano cluster (Connor & Conway, 2000). The distributed style of volcanism that forms such clusters is sourced from a spatially broad and long-lived (hundreds of thousands to hundreds of millions of years) magma generation event that intermittently sends magma to the surface of the crust. As small volcanic vents (<10 km length on Mars) are most likely formed from the eruption of a single dike, and thus construct "monogenetic" volcanoes (Kereszturi & Németh, 2013), vent morphology often preserves dike characteristics (Tadini et al., 2014; G. Valentine & Gregg, 2008). Specifically, vent orientation serves as a proxy for dike direction as elongate vents are likely aligned with the direction of the underlying dike. We now use the catalog to investigate spatial, temporal, and morphologic trends of distributed-style volcanism across Tharsis.

4.0.0.1 Confidence in some vents On the main flanks of the large volcanoes of Tharsis, only Olympus Mons and Arsia host a significant number of volcanic vents. On the flanks of Olympus Mons, 29 vents are mapped up to the elevation of 16.8 km. In a previous version of this catalog (Bleacher et al., 2010), additional potential vent features were included on the flanks of Olympus Mons that had a morphology consistent with the vent morphology definition. An alternative interpretation of these structures on the Olympus Mons flank is that low-shield-like volcanic rises are points along lava flows where lava broke out of a tube or channel structure at a break in slope (Bleacher, Greeley, Williams, Werner, et al., 2007; Peters & Christensen, 2017; P. Mouginis-Mark, 2018). These structures would then be analogous to secondary vents seen on Etna lava flows (Calvari & Pinkerton, 1998). At Olympus Mons, features are removed from the Bleacher et al. (2010) catalog where a channel or topographic ridge is observable immediately upslope and in-line with the vent feature. Only locations with clear depressions at an isolated topographic rise are included in the catalog presented in this paper, though these vents might still be constructional features from channelized lava flows.

In the lava plains of Tharsis, including Daedalia Planum and regions east of the Tharsis Montes, chains of closely-spaced pit craters lie at the tops of low-sloping, conical edifices that are morphologically equivalent to low shields. These "small shields" are formed by relatively short (1-2 km in length) lava flows from the pit craters. While they fit the criteria as a volcanic vent, it is likely that these vents are also secondary vents (Calvari & Pinkerton, 1998), forming from the outflow of lava from a pressurized lava tube. Evidence for this is ambiguous; while these curvilinear chains of pit craters follow the downward trending orientation of neighboring lava flows, this orientation is also roughly radial from nearby large volcanoes, specifically Arsia and Pavonis. Because of this ambiguity, these features remain in the catalog as they are morphologically indistinguishable from other volcanic vents.

4.1 Temporal trends of distributed volcanism at Tharsis

Several prior studies have modeled the ages of distributed volcanoes around Tharsis, either by mapping crater populations at individual volcanoes (e.g., Hauber et al., 2011; Brož, 2010) or by mapping craters across volcanic fields composed of distributed volcanoes. Results from different geochronology studies are similar on a region-by-region basis, and are most similar in regions where vents are very recent (Figure 10). Two regions in this study have not had any vents previously dated: the Fortuna region and the potential vents in Daedalia Planum.

The oldest vent fields in the Tharsis Volcanic Province are at its periphery. The oldest vent cluster currently at the surface within Tharsis is Syria Planum, whose earliest vents were emplaced over 3 billion years ago (Richardson et al., 2013; Hauber et al., 2011; Baptista et al., 2008). Syria Planum's main phase of activity was during the Hesperian to Early Amazonian (Richardson et al., 2013; Baptista et al., 2008) or throughout the Amazonian with the majority of vents being emplaced before 1 Ga (Hauber et al., 2011; Brož, 2010). The second oldest cluster of vents is identified as Tempe-Mareotis whose activity likely spanned the last billion years, though Manfredi (2012) mapped shields in the area as old as 2.3 Ga. Additionally, the adjacent Labeatis Mons has been dated

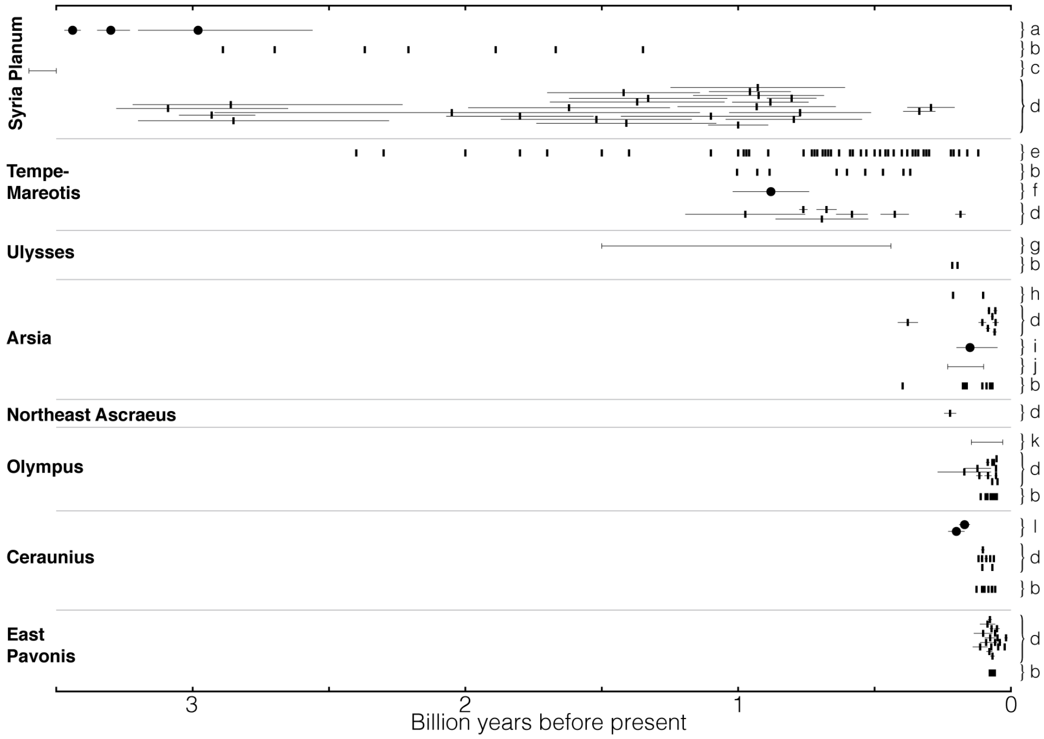

Figure 10. Chart of previously dated volcanic edifices and terrains that spatially overlap with vents in this catalog. Geochronology based on crater retention indicates a long history of distributed style volcanism in Tharsis, from >3 Ga to 10s Ma. Vertical bars are modeled ages for individual, distributed-style volcanic edifices and flows; circles are age models of terrains composed of multiple volcanic edifices; horizontal bars illustrate reported uncertainty; horizontal lines with barred ends are ages reported as a range. *a) Richardson et al. (2013), b) Brož (2010), c) Baptista et al. (2008), d) Hauber et al. (2011), e) Manfredi (2012), f) Plescia (1981), g) Brož and Hauber (2012), h) Werner (2009), i) Richardson et al. (2017), j) Bleacher et al. (2009), k) Basilevsky et al. (2006), l) Christoph and Garry (2017).*

by Neesemann et al. (2010) to be 822 Ma in age, which is within age ranges found for activity within the Tempe-Mareotis region. The only other cluster with dated edifices that might be >1 Ga in age are a cluster of cones within the Ulysses region of the catalog, which was given an age range by dating stratigraphically bounding units by Brož and Hauber (2012).

All other vent regions in the catalog that have previously been the targets for age-dating (Arsia, Northeast Ascreaus, Olympus, Ceraunius, and East Pavonis) have edifices whose ages are all younger than 500 Ma, with the majority of all dated volcanoes or regions being <250 Ma in age. These dates are similar to the ages of the rift apron lavas adjacent to the Tharsis Montes (Werner, 2009; Crown & Ramsey, 2015; Giacomini et al., 2009). All of these late Amazonian-aged regions of vents are within 1000 km of the Tharsis Montes or Olympus Mons. In these regions, the lack of volcanic edifices identified as being >500 Ma indicates either the absence of older distributed volcanism or that the rift apron deposits were voluminous enough to completely bury older edifices, potentially as far away as Ceraunius Fossae. Neither of these hypotheses are tested here, though an absence of older distributed volcanism near the Tharsis Montes would mean that virtually all volcanism during the period of initial edifice formation was constrained to the central volcanoes. This is in line with a lack of observed distributed vents in the vicinity of Alba Mons, even though it has not been volcanically resurfaced in the last 1 Ga (Werner, 2009). If vent burial is the cause of missing older vents in these regions, it would almost certainly be due to burial by rift apron lavas, as they completely cover the present landscape (Tanaka et al., 2014), instead of other distributed volcanic deposits, as regions with older volcanoes had activities spanning over 1 billion years without burying their oldest vents (Richardson et al., 2013).

4.2 Spatial trends of distributed volcanism at Tharsis

Dozens of distributed volcanic vents are observed to the east of each of the central volcanoes in Tharsis (Olympus, Pavonis, Ascraeus, Arsia). These populations lay in contrast to a virtual absence of volcanic vents to the west of the same volcanoes. Within 500 km of the Tharsis Montes, only about 50 vents are identified to the northwest, compared to approximately 400 small vents to the southeast within the same distance. This dichotomy could exist for a number of reasons including northwestern ice deposits on each shield volcano flank, which could have buried or eroded vents, more efficient burial by rift apron lavas, or simply because volcanic vents were not created as frequently to the northwest of the Tharsis Montes.

The dozens of vents adjacent to the flanks of the large volcanoes also contrast with the lack of distributed vents on their flanks. Discounting vents that are present on rift aprons, only Arsia Mons hosts volcanic vents at its summit. If the potential vents at Olympus Mons are also the result of distributed volcanism instead of fanned out lava flow features, then Olympus Mons is the only large volcano in Tharsis to host volcanic vents on its flanks. Pavonis, Ascraeus, and Alba Mons on the other hand do not appear to have small volcanic vents on their main edifices. On the main flanks of these volcanoes instead, circular graben indicate the presence of large circumferential dikes within the volcanoes, consistent with an interpretation that magma flowed first through central magma chambers before further ascending to the surface (Montési, 2001).

The vent-free flanks of the Tharsis Montes and evidence of large circumferential dikes within them indicates that during formation, magma flux was sustained at a high rate. Distributed vents on central volcanoes are typical in systems where magma flux gradually waned and a centralized magma chamber was no longer sustainable (Bleacher & Greeley, 2008; Rowland & Walker, 1990; Rowland, 1996). While a pressurized magma chamber is present in the subsurface, ascending dikes from below the chamber will be deflected toward the chamber, creating a “shadow zone” where distributed-style volcan-

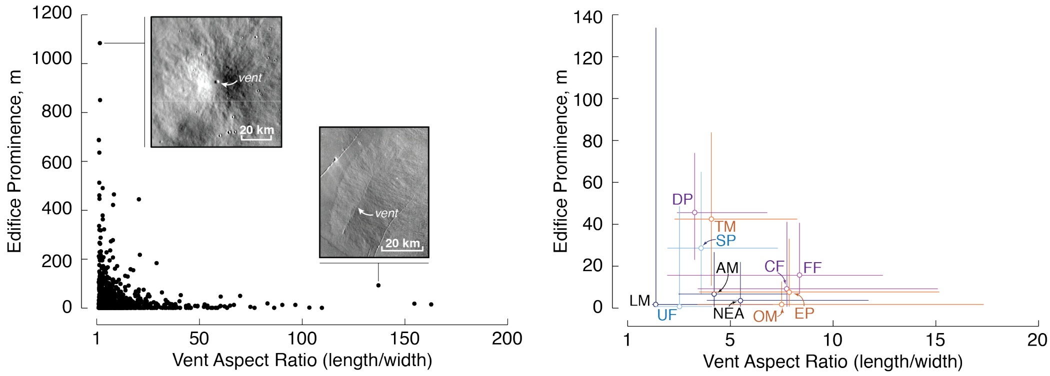

Figure 11. (left) Highly prominent edifices have equant vents and highly elongate vents do not construct high edifices. The left example vent (vent #381, -10.31°N -101.45°E) is at the regional summit of Syria Planum. The right example (vent #834, 0.88°N -104.84°E) constructs a low shield east of Pavonis Mons. Examples use the THEMIS daytime image mosaic. (right) Median values of aspect ratio and prominence for vents in each region. Vertical and horizontal bars are drawn to 25th and 75th percentiles of aspect ratio and prominence. Axis scale on the right is larger than the left. Region acronyms and colors are the same as Figure 3.

ism is absent above the chamber (Karlstrom et al., 2015). We interpret that the flanks of the Tharsis Montes, when they were initially constructed, were within this "shadow zone," where magma was delivered to the surface from a chamber instead of directly from a lower source at the base of the martian crust. Atop the younger lava apron units of the Tharsis Montes, within the Arsia Mons summit caldera, and potentially on the Olympus Mons flanks, the presence of vents on top of flank lava flows does indicate that magma productivity waned before entirely ceasing.

4.3 Morphologic trends of distributed volcanism at Tharsis

4.3.1 Vent dimensions

Among the vent population, a relationship exists between vent aspect ratio and prominence (Figure 11, left) where highly elongate vents do not form a tall edifice and only equant or nearly equant vents form very high, >500 m edifices. These two measures are not related by a linear trend; instead highly elongate vents and highly prominent vents are end members, while 81% of vents are low (<100 m prominent) and have aspect ratios <24. End member populations of highly prominent or elongate vents have virtually no overlap as seen in Figure 11 (left); the most elongate vent with a prominence ≥100 m has an aspect ratio of 29, while the most prominent vent with a ≥24 aspect ratio is 184 m high.

The evolution of monogenetic volcanic vent shape and its morphologic relationship to shallow conduit geometry has been studied at diverse locations including Hawaii (Parcheta et al., 2015), Iceland (Reynolds et al., 2017), and the Canary Islands (Dóniz-Páez, 2015). Often eruptions in volcanic fields begin as elongate fissure eruptions, and through time evolve into one or several isolated vents along the axis of the fissure (Witt et al., 2018; Mitchell, 2005). The distribution of aspect ratios and prominences in this catalog is in agreement with this terrestrially observed trend. Because most of these small volcanoes were constructed from a single period of eruptions, it is expected that the elongate end member vents were likely short-lived compared to prominent and circular vents, which would have been constructed from sustained eruptions that led to the development of a concentrated, circular vent.

Plotting the spread of aspect ratio and prominence for different regions within Tharsis (Figure 11, right) shows that each region contains a variety of vent and associated edifice morphologies. No one region comprises only very long vents or very high structures and the spread in aspect ratio and prominence of each region of vents overlaps with all other vents. There is a temporal trend for prominence, where the geologically recent clusters with more than several vents (Northeast Ascraeus, Olympus, East Pavonis, Ceraunius, Ulysses, and Arsia) all have median prominence values of <10 m, while older regions with more than several vents (Syria, Fortuna, and Tempe Mareotis) all have median prominences of 29, 16, and 51 m respectively. A corresponding division does not exist for aspect ratio values. If prominence is a proxy for volume erupted and aspect ratio a proxy for eruption duration, this indicates older volcano clusters would have had eruptions with greater average volume flux than more recent volcanic centers.

4.3.2 Vent orientations

In each region of Tharsis, elongate vents have preferential orientations that produce modal trends as illustrated in Figure 7b. Away from the central volcanoes, vent orientations are aligned with surrounding graben sets. Near some central volcanoes, radial trends are present in small vent orientation within 500 km of the volcano summit (Figure 8. This is most remarkable for vents near Olympus Mons, which include potential vents on the Olympus Mons flanks and a cluster of vents adjacent to its eastern flank. A plurality of these vents are oriented within 10° of radial to the Olympus summit. Similar but less pronounced trends are seen at Arsia and Ascraeus Mons. Pavonis Mons, however, does not appear to have a substantial population of nearby radial vents, though distant vents are radially oriented. These distant, radial vents include dozens of vents within Syria Planum and vents that are parallel to graben sets in Tempe Mareotis. These radially oriented populations of vents are consistent with the identification of the Pavonis area as a dominant tectonic center during the Noachian and Hesperian Periods (Anderson et al., 2001).

4.4 Two end members for distributed volcanism at Tharsis

We find that the clustered products of distributed volcanism in Tharsis are governed by two regional-scale, preexisting feature types: large volcanoes and graben systems. Distributed volcanism over virtually all of Tharsis directly overlies or lies adjacent to these features and the presence of either large volcanoes or regional graben systems creates end-member styles of distributed volcanism. These end-member styles, either large volcano- or fossae-dependent volcano clusters, produce small volcanoes that have characteristic vent orientations, intervent alignments, and prominences.

4.4.1 Central volcano-dependent volcanism

Clusters of distributed volcanoes up to 1,000 km from summits of the central volcanoes, Olympus Mons, Arsia Mons, and Ascraeus Mons, have vent orientations that are radially aligned with respect to each central volcano (Figure 7). This radial pattern is most apparent to the east of Olympus Mons (Figure 12 *left*), but is less clear at the Tharsis Montes, where vents along the axis of the Tharsis Montes and on top of the rift apron deposits are aligned radial to Arsia and Ascreaus (and coincidentally are oriented parallel to the axis). To the east of the Tharsis Montes, vents are instead mostly oriented parallel to the Tharsis Montes except for vents that are adjacent to the volcanoes. If both vents along the axis and off-axis were essentially co-temporal, this shows a limit to the ability of central volcanoes to govern vent orientation.

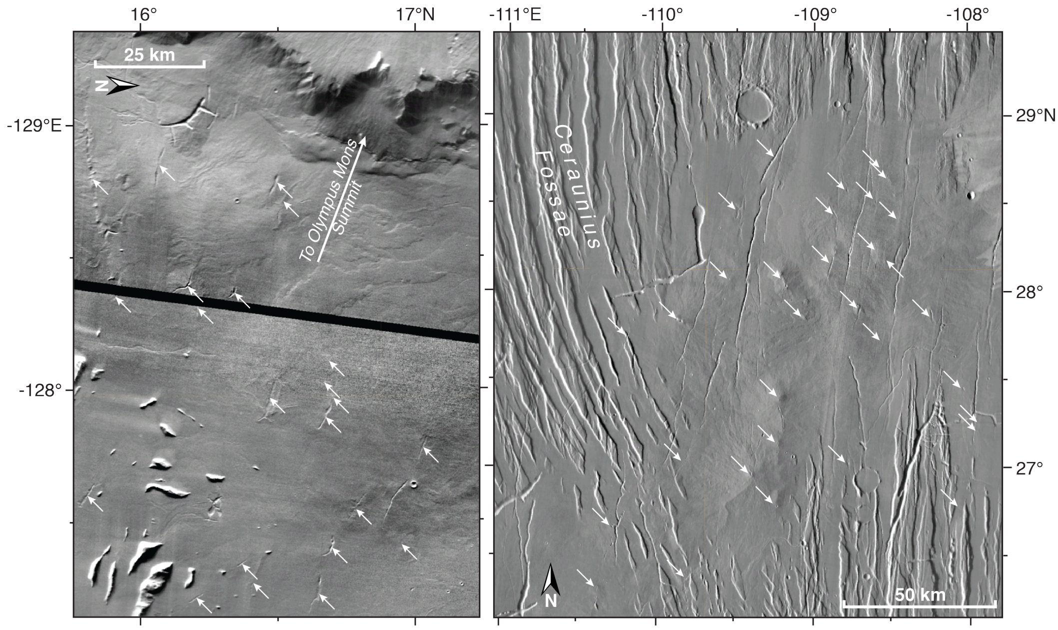

Figure 12. (left) Vents to the east of Olympus Mons (shown) and around Ascraeus and Arsia Mons are oriented radially away from the summit of the central volcanoes. In this view, several elongate depressions (most 5-15 km in length) at the summit of low shields are pointed radially or subradially to the Olympus summit calderas. The flanks of Olympus are seen at the top edge of the figure. (right) Dominating regional fossae, including Ceraunius (shown here), Tempe, and Mareotis are observed to transition to smooth plains units, which host clusters of volcanic vents. Vents on such smooth plains are elongate in the direction parallel to the strike of the surrounding grabens. Vents in this figure are again atop low shields and are oriented either north-northwest, parallel to the graben to the west, or north by east, aligned with graben to the north and south. Basemap is THEMIS daytime mosaic.

Intervent alignments are less clearly linked to central volcanoes. At Olympus Mons, intervent alignments of near-neighbor vents show no clear preferential orientation (Figure 9, *left*). Intervent alignments to the northeast of Ascraeus Mons do show a broad modal preference for NE-E orientation, which might be an effect of the presence of Ascraeus. This pattern is at least more radial than intervent alignments to the east of Pavonis Mons, which are predominantly aligned parallel to the axis of the Tharsis Montes.

Evidence for large magmatic dikes that propagated radially over 1,000 km from Olympus Mons have been identified (P. J. Mouginis-Mark & Wilson, 2019), showing clearly that shallow (<10 km depth) magma injection is able to align radially to a pressurized magma chamber on Tharsis. The small vent orientations in the catalog could have similarly been a product of radially-aligned dikes, either due to the mass load of the large central volcanoes or from co-temporal magma chambers. At Olympus Mons, injection of a magma chamber at ∼210 Ma occurred (Chadwick et al., 2015), which is co-temporal to the emplacement of nearby vents (Figure 10). However, the lack of a radial preference for intervent alignments at Olympus Mons suggests that feeder dikes for these small volcanoes were not radially propagated. One expected outcome of radially propagated dikes would be the construction of multiple vents along single dikes (Gudmundsson, 1995; Hartley et al., 2018), which would produce a modal intervent alignment direction similar to the preferred vent orientation. Instead, the lack of this preferred alignment direction at Olympus implies more or less vertical dike ascent where dikes re-oriented during ascent to radially align with the central volcano (Gautneb & Gudmundsson, 1992; Karlstrom et al., 2009).

4.4.2 Fossae-dependent volcanism

Clusters of distributed volcanoes spatially associated with Ceraunius Fossae, Tempe Fossae, and Mareotis Fossae have highly modal vent orientations that are clearly aligned with surrounding graben sets. Additionally, vent alignments at Ceraunius Fossae are predominantly N-S, co-aligned with grabens and the largest mode of intervent alignments at Tempe-Mareotis (36% of 73 alignments between 30-70°N) are co-aligned with E-NE grabens. Alignments in these end-member example regions are often co-aligned with vent orientation, which is evidence that dikes in these areas ascended parallel to graben sets.

As described above, volcanoes in Ceraunius are significantly younger than the surrounding fossae. Recent (<500 Ma) graben-aligned dike ascent could be explained, in the absence of continued faulting during the late Amazonian, by deep penetration of crustal fractures associated with Ceraunius Fossae. If deep dikes were instead controlled by deviatoric stress and only exploit preexisting fractures at shallower depths, *en echelon* vents and a difference between intervent alignments and vent orientation would be observed. Examples of this pattern are found in the Ulysses region, where the modal vent orientation is counter-clockwise rotated from the modal vent alignment direction.

4.4.3 Non-end member distributed volcanism

Most distributed volcanism during the history of Tharsis would have been affected by both large fractures and large volcanoes, given the prevalence of both features over the Tharsis surface. As an example, magma at Northeast Ascreaus might have ascended in a regime riddled with pre-existing fractures and adjacent to a large shield volcano. Volcanic vents in this region show a clockwise rotation from modal intervent alignment to modal vent orientation. This could be attributed to dikes that were initially co-aligned with deep underlying NE-SW fractures (Anderson et al., 2001) that ascended and rotated to radially orient with respect to Ascraeus Mons before eruption.

Syria Planum is the volcano cluster most isolated from large volcanoes and graben sets, despite regionally being surrounded by Noctis Labyrinthus. On this plateau, vents

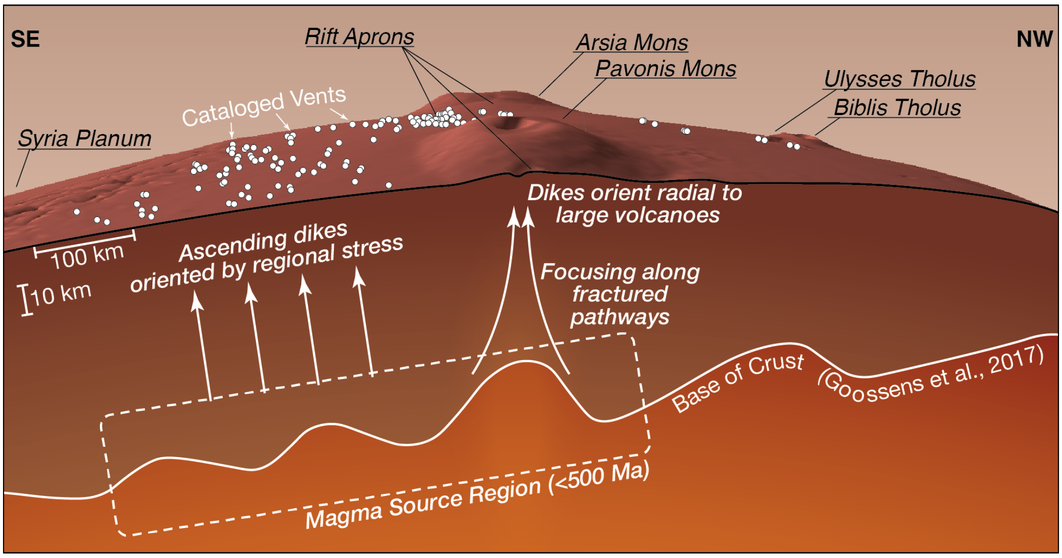

Figure 13. Perspective view and cross section across Pavonis Mons looking south. Vents in this catalog are labeled at the surface as white circles. We hypothesize the presence of a broad magma source region that fed recently (<500 Ma) emplaced volcanic vents along the Tharsis Montes axis and to its east. In the east, ascending dikes ascended without significant focusing and predominantly oriented parallel to the axis. Focusing of magma under the Tharsis Montes enabled emplacement of rift apron lavas and some radially oriented distributed vents near each large volcano. The solid white curve within the martian interior is a model of the base of the crust by Goossens et al. (2017). Vertical exaggeration is 3x and the crust is thickness exaggeration of 6x.

are preferentially oriented NW, back towards the center of Tharsis. Based on intervent alignments, Richardson et al. (2013) identified this direction as a primary orientation affecting magma ascent and attributed it to a tectonic center near Pavonis Mons hypothesized by Anderson et al. (2001). Based on the burial of local sets of local grabens by Syria Planum volcanism (Richardson et al., 2010), cracks and/or tectonic stress that enabled this NW-SE vent orientation would have been present before the last volcanic activity at Syria Planum during the early Amazonian. It is possible that Hesperian volcanism in southern Syria Planum (3.2-3.4 Ga, (Richardson et al., 2013)) was cotemporal to the Hesperian tectonic center near Pavonis Mons (Anderson et al., 2001). If this was the case, vent orientation might be aligned NW-SE due to ongoing deviatoric stress during formation of the volcanic field.

4.5 Latest volcanism at the Tharsis Montes

The spatial distribution and morphologies of young (<500 Ma) volcanic vents adjacent to the Tharsis Montes (primarily the Arsia, East Pavonis, and Northeast Ascraeus regions) lead us to the interpretation that the most recent distributed volcanism near the Tharsis Montes was due to a single broad magma source region. Here we outline the evidence and implications of this hypothesis.

Unlike distributed volcanism that occurs as the waning stage of central-vent volcanism (*e.g.*, cones at Mauna Kea, Hawaii (Kervyn et al., 2012; Settle, 1979)), recent Tharsis Montes volcanism did not produce small vents on the main flanks of the volcanoes, nor do distributed volcanoes surround the Tharsis Montes. Instead, of the 325 volcanic vents in this catalog within 500 km of the axis of the Tharsis Montes (ad-hoc defined as a great circle line from the summit of Ascraeus Mons to Arsia Mons), 269 of the vents, 83%, lie to the east of axis.

In addition to the decentralized spatial distribution of vents, orientations of vents are also in disagreement with a Tharsis Montes-centered magmatic provenances for recent distributed volcanism. Instead of orienting radially to each large volcano, the majority of volcanic vents in the Arsia, East Pavonis, and Northeast Ascraeus regions are oriented NE-SW (Figure 7), parallel to the Tharsis Montes Axis. Volcanic vents along the rift aprons of each of the large shields are oriented both parallel to the axis and radial to the large shields, similar to volcanic vents along the spreading center of central Iceland (Gudmundsson, 1995).

Late Amazonian volcanism in the region surrounding the Tharsis Montes includes the rift apron deposits and distributed volcanic vents (Werner, 2009; Crumpler & Aubele, 1978). We suggest that both features can be explained by a single magmatic source region (Figure 13). In this model, distributed volcanism away from the Tharsis Montes is a product of unfocused magma ascending vertically through intact bedrock. The orientations and alignments of vents to the east of the Tharsis Montes are primarily NE-SW, which might have been determined from pre-existing fractures with a similar orientation to grabens exposed northeast at Tempe Terra and the chasmata of the Tharsis Montes.

We interpret the rift apron deposits abutting the large volcanoes to be products of the same broad magmatic source, enabled by the extensive NE-SW fracturing of the Tharsis Montes (Crumpler & Aubele, 1978; Bleacher, Greeley, Williams, Cave, & Neukum, 2007). When magma underlies a heavily fractured crust it is sometimes more able to ascend due to the presence of pre-existing pathways and lack of rigid rock layers that inhibit vertical dike propagation. For example, evidence of a positive correlation between permeability and magma transport seen on Earth, including the Southwest Indian Ridge where magma laterally focuses under rigid layers to relatively narrow extraction zones (Montési et al., 2011). Additionally, magma flux at the distributed-style Springerville Volcanic Field (Arizona, USA) likely does not undergo much lateral focusing but is still correlated to density anomalies in the crust where high-density crustal blocks inhibit magma ascent (Deng et al., 2017).

If magma flux was high enough, late Amazonian focusing of magma underneath the Tharsis Montes would have created magma chambers to source the rift apron lavas, which for the most part have no identifiable vent sources. Evacuation of magma chambers in depositing these lava flows has contributed to the basaltic calderas at the summits of each shield volcano. It is possible that the latest stage of rift apron emplacement did produce more prominent, smaller volcanoes along the rift aprons, similar to Mauna Kea waning volcanism as suggested by Bleacher et al. (2009). Late stage magmatism from this focused activity might also have produced the highest volcano cluster on Tharsis within the Arsia Mons Caldera. Lastly, significant magma focusing would have increased the bulk density within the cores of the fractured Tharsis Montes. Evidence of this is seen in the Moho model of Goossens et al. (2017), where the crust thickens under each large volcano but then rapidly thins under each Tharsis Montes summit (Figure 13). We propose an alternative explanation of this result: that mass concentrations of unfractured basalt are present within each central volcano instead of uplifted mantle and that these basalts fed the rift apron lavas.

5 Conclusions

We present a catalog of 1106 small volcanic vents identified within Tharsis Volcanic Province that include morphologic measurements for each cataloged vent including vent dimension, orientation, and prominence. Vent lengths range from 71 m to 51 km, widths range from 40 m to 3.1 km, and most edifices associated with vents have prominences of <100 m. Our measurements indicate that 90% of vents are elongate (*i.e.*, have lengths a factor of at least 1.5 greater than their widths). Very elongate vents do not have high topographic prominences, while prominent volcanoes do not have very elongate vents. Small, distributed-style volcanoes are found throughout Tharsis, though they generally form clusters near large volcanoes or among large graben sets. Possible vents on the flanks of large volcanoes are only seen on Olympus Mons, but these might be landforms constructed from lava flows breaking out from channel systems. Only Arsia Mons hosts small vents at its summit. Distributed-style volcanism is therefore not a universal conclusion to main edifice construction of large shield volcanoes.

Distributed-style volcanism has produced volcanic vents over surfaces of all ages within Tharsis, from the late Noachian to potentially just several million years ago. Older vent clusters with volcanic eruption ages of >1 Ga are found on the eastern outskirts of Tharsis in the Tempe-Mareotis region and Syria Planum. Vents in the Tharsis interior have reported ages <500 Ma and the majority are spatially adjacent to the Tharsis Montes, Olympus Mons, and Ceraunius Fossae. Over 700 vents within the catalog are within regions of volcanism that developed in the latest 500 Ma.

Two end members of distributed-style volcanism are defined by regionally governing features: large volcano-dependent volcanism and fossae-dependent volcanism. Vent orientations and intervent alignments are ideally oriented radially to large volcanoes and parallel to regional graben sets. Fossae-dependent volcanism is more unambiguously expressed at the Tharsis Volcanic Province, while central volcano-dependent volcanism is most clearly expressed adjacent to the Eastern base of Olympus Mons.

We interpret that there is a genetic link between distributed volcanoes to the east and between the Tharsis Montes and the rift apron deposits. In this scenario, a broad magma source region, centered to the east of the Tharsis Montes would have fed magma to the surface over the last 500 Ma. Magma beneath the Tharsis Montes would have focused through axial crustal fractures, efficiently ascended, and emplaced the large rift apron deposits and distributed vents on top of the rift aprons. Magma to the east instead ascended less efficiently through less fractured crust, producing distributed-style volcanism only.

Acknowledgments

The vent catalog database and python code that analyzed raw measurements to construct the vent catalog is available at https://doi.org/10.5281/zenodo.4275144 (Richardson et al., 2020). The enhanced vent catalog is also available as supplemental information included with this manuscript. Mapping and data analysis were supported by the NASA Mars Data Analysis Program, grant #NNX14AN02G. Work by J. Richardson was also supported by NASA under award #80GSFC17M0002. J. Richardson thanks his lab's writing support group and valuable feedback from Sarah Sutton.

References

Anderson, R. C., Dohm, J. M., Golembek, M. P., Haldemann, A. F. C., Franklin, B. J., Tanaka, K. L., ... Peer, B. (2001). Primary centers and secondary concentrations of tectonic activity through time in the western hemisphere of Mars. *Journal of Geophysical Research*, *106*(E9), 20,520–563,585. doi: 10.1029/2000JE001278

Baptista, A. R., Mangold, N., Ansan, V., Baratoux, D., Lognonné, P., Alves, E. I., ... Neukum, G. (2008). A swarm of small shield volcanoes on Syria Planum, Mars. *Journal of Geophysical Research*, *113*(E9), E09010. doi: 10.1029/2007JE002945

Basilevsky, A. T., Werner, S. C., Neukum, G., Head, J. W., Van Gasselt, S., Gwinner, K., & Ivanov, B. A. (2006). Geologically recent tectonic, volcanic and fluvial activity on the eastern flank of the Olympus Mons volcano, Mars. *Geophysical Research Letters*, *33*(13), 5–8. doi: 10.1029/2006GL026396

Beyer, R. A., Alexandrov, O., & McMichael, S. (2018). The ames stereo pipeline: Nasa's open source software for deriving and processing terrain data. *Earth and Space Science*, *5*(9), 537–548.

Bleacher, J. E., Glaze, L. S., Greeley, R., Hauber, E., Baloga, S. M., Sakimoto, S. E., … Glotch, T. D. (2009). Spatial and alignment analyses for a field of small volcanic vents south of Pavonis Mons and implications for the Tharsis province, Mars. *Journal of Volcanology and Geothermal Research*, *185*(1-2), 96–102. doi: 10.1016/j.jvolgeores.2009.04.008

Bleacher, J. E., & Greeley, R. (2008). Relating volcano morphometry to the developmental progression of Hawaiian shield volcanoes through slope and hypsometric analyses of SRTM data. *Journal of Geophysical Research*, *113*, B09208. doi: 10.1029/2006JB004661

Bleacher, J. E., Greeley, R., Williams, D. A., Cave, S. R., & Neukum, G. (2007). Trends in effusive style at the Tharsis Montes, Mars, and implications for the development of the Tharsis province. *Journal of Geophysical Research*, *112*(E9), E09005. doi: 10.1029/2006JE002873

Bleacher, J. E., Greeley, R., Williams, D. A., Werner, S. C., Hauber, E., & Neukum, G. (2007). Olympus Mons, Mars: Inferred changes in late Amazonian aged effusive activity from lava flow mapping of Mars Express High Resolution Stereo Camera data. *Journal of Geophysical Research: Planets*, *112*(E4), E04003. doi: 10.1029/2006JE002826

Bleacher, J. E., Richardson, J. A., Richardson, P. W., Glaze, L. S., Baloga, S. M., Greeley, R., … Lillis, R. J. (2010). Updates to the Catalog of Tharsis Province Small Volcanic Vents, Mars. In *Lunar and Planetary Science Conference, abs. 1615.*

Bohnenstiehl, D. W. R., Howell, J. K., White, S. M., & Hey, R. N. (2012). A modified basal outlining algorithm for identifying topographic highs from gridded elevation data, Part 1: Motivation and methods. *Computers and Geosciences*. doi: 10.1016/j.cageo.2012.04.023

Brož, P. (2010). *Plains volcanism in Tharsis region on Mars: Ages and Rheology of Eruption Products* (Unpublished doctoral dissertation). Charles University in Prague.

Brož, P., & Hauber, E. (2012). A unique volcanic field in Tharsis, Mars: Pyroclastic cones as evidence for explosive eruptions. *Icarus*, *218*(1), 88–99. doi: 10.1016/j.icarus.2011.11.030

Calvari, S., & Pinkerton, H. (1998). Formation of lava tubes and extensive flow field during the 1991–1993 eruption of mount etna. *Journal of Geophysical Research: Solid Earth*, *103*(B11), 27291–27301.

Carr, M. H. (1973). Volcanism on Mars. *Journal of Geophysical Research*, *78*(20), 4049–4062. doi: 10.1029/JB078i020p04049

Carr, M. H. (1974). Tectonism and volcanism of the Tharsis region of Mars. *Journal of Geophysical Research*, *79*(26), 3943–3949. doi: 10.1029/JB079i026p03943

Cebriá, J. M., Mart\'\in-Escorza, C., López-Ruiz, J., Morán-Zenteno, D. J., & Martiny, B. M. (2011). Numerical recognition of alignments in monogenetic volcanic areas: Examples from the Michoacán-Guanajuato Volcanic Field in Mexico and Calatrava in Spain. *Journal of Volcanology and Geothermal Research*, *201*(1–4), 73–82. doi: 10.1016/j.jvolgeores.2010.07.016

Chadwick, J., McGovern, P., Simpson, M., & Reeves, A. (2015). Late Amazonian subsidence and magmatism of Olympus Mons, Mars. *Journal of Geophysical Research: Planets*.

Christensen, P., Jakosky, B., Kieffer, H., Malin, M., McSween, H., Nealson, K., …

Ravine, M. (2004). The Thermal Emission Imaging System (THEMIS) for the Mars 2001 Odyssey Mission. *Space Science Reviews*, *110*(1), 85–130. doi: 10.1023/B:SPAC.0000021008.16305.94
Christoph, J. M., & Garry, W. B. (2017). Spatial and Temporal Relationships Among Low Shield Volcanoes in the Ceraunius Fossae Region of Tharsis: The Last Gasp of Martian Volcanism. In *Lunar and Planetary Science Conference, abs. 2798* (Vol. 48).
Connor, C. B., & Conway, M. F. (2000). Basaltic volcanic fields. In H. Sigurdsson (Ed.), *Encyclopedia of volcanoes* (pp. 331–343). San Diego, CA: Academic Press.
Crown, D. A., & Ramsey, M. S. (2015). *Morphologic and thermophysical characteristics of lava flows southwest of Arsia Mons, Mars.* doi: 10.1016/j.jvolgeores.2016.07.008
Crumpler, L. S., & Aubele, J. C. (1978). Structural evolution of Arsia Mons, Pavonis Mons, and Ascreus Mons: Tharsis region of Mars. *Icarus*, *34*(3), 496–511. doi: 10.1016/0019-1035(78)90041-6
Deng, F., Connor, C. B., Malservisi, R., Connor, L. J., White, J. T., Germa, A., & Wetmore, P. H. (2017). A Geophysical Model for the Origin of Volcano Vent Clusters in a Colorado Plateau Volcanic Field. *Journal of Geophysical Research: Solid Earth*, *122*(11), 8910–8924. doi: 10.1002/2017JB014434
Dóniz-Páez, J. (2015). Volcanic geomorphological classification of the cinder cones of Tenerife (Canary Islands, Spain). *Geomorphology*, *228*, 432–447.
Fernández, C., & Ramírez-Caballero, I. (2019). Evaluating transtension on Mars: The case of Ulysses Fossae, Tharsis. *Journal of Structural Geology*. doi: 10.1016/j.jsg.2018.05.009
Gautneb, H., & Gudmundsson, A. (1992). Effect of local and regional stress fields on sheet emplacement in West Iceland. *Journal of Volcanology and Geothermal Research*, *51*(4), 339–356. doi: 10.1016/0377-0273(92)90107-O
Giacomini, L., Massironi, M., Martellato, E., Pasquarè, G., Frigeri, A., & Cremonese, G. (2009). Inflated flows on daedalia planum (mars)? clues from a comparative analysis with the payen volcanic complex (argentina). *Planetary and Space Science*, *57*(5-6), 556–570. doi: 10.1016/j.pss.2008.12.001
Golombek, M. P., Tanaka, K. L., & Franklin, B. J. (1996). Extension across Tempe Terra, Mars, from measurements of fault scarp widths and deformed craters. *Journal of Geophysical Research E: Planets*. doi: 10.1029/96JE02709
Goossens, S., Sabaka, T. J., Genova, A., Mazarico, E., Nicholas, J. B., & Neumann, G. A. (2017). Evidence for a low bulk crustal density for mars from gravity and topography. *Geophysical research letters*, *44*(15), 7686–7694.
Greeley, R. (1977). Basaltic "plains" volcanism. In R. Greeley & J. S. King (Eds.), *Volcanism of the eastern snake river plain, idaho: A comparative planetary geology guidebook, nasa cr-154621* (pp. 23–44). Washington, D. C.: NASA.
Gudmundsson, A. (1995). Infrastructure and mechanics of volcanic systems in Iceland. *Journal of Volcanology and Geothermal Research*, *64*(1-2), 1–22. doi: 10.1016/0377-0273(95)92782-Q
Halevy, I., & Head III, J. W. (2014). Episodic warming of early Mars by punctuated volcanism. *Nature Geoscience*.
Hartley, M. E., Bali, E., Maclennan, J., Neave, D. A., & Halldórsson, S. A. (2018, feb). Melt inclusion constraints on petrogenesis of the 2014–2015 Holuhraun eruption, Iceland. *Contributions to Mineralogy and Petrology*, *173*(2), 10. doi: 10.1007/s00410-017-1435-0
Hauber, E., Bleacher, J., Gwinner, K., Williams, D., & Greeley, R. (2009). The topography and morphology of low shields and associated landforms of plains volcanism in the Tharsis region of Mars. *Journal of Volcanology and Geothermal Research*, *185*(1–2), 69–95. doi: 10.1016/j.jvolgeores.2009.04.015
Hauber, E., Brož, P., Jagert, F., Jodł˜owski, P., & Platz, T. (2011). Very recent

and wide-spread basaltic volcanism on Mars. *Geophysical Research Letters*, *38*, L10201. doi: 10.1029/2011GL047310

Hauber, E., & Kronberg, P. (2001). Tempe Fossae, Mars: A planetary analogon to a terrestrial continental rift? *Journal of Geophysical Research E: Planets*. doi: 10.1029/2000JE001346

Head, J. W., Crumpler, L. S., Aubele, J. C., Guest, J. E., & Saunders, R. S. (1992). Venus volcanism: Classification of volcanic features and structures, associations, and global distribution from Magellan data. *Journal of Geophysical Research: Planets*, *97*(E8), 13153–13197.

Jaeger, W. L., Keszthelyi, L. P., Skinner Jr, J., Milazzo, M., McEwen, A. S., Titus, T. N., ... others (2010). Emplacement of the youngest flood lava on mars: A short, turbulent story. *Icarus*, *205*(1), 230–243.

Karlstrom, L., Dufek, J., & Manga, M. (2009). Organization of volcanic plumbing through magmatic lensing by magma chambers and volcanic loads. *Journal of Geophysical Research: Solid Earth*, *114*(B10). doi: 10.1029/2009JB006339

Karlstrom, L., Wright, H. M., & Bacon, C. R. (2015). The effect of pressurized magma chamber growth on melt migration and pre-caldera vent locations through time at Mount Mazama, Crater Lake, Oregon. *Earth and Planetary Science Letters*, *412*, 209–219. doi: 10.1016/j.epsl.2014.12.001

Kerber, L., Head, J. W., Madeleine, J.-B., Forget, F., & Wilson, L. (2012). The dispersal of pyroclasts from ancient explosive volcanoes on mars: Implications for the friable layered deposits. *Icarus*, *219*(1), 358–381.

Kereszturi, G., & Németh, K. (2013). Monogenetic Basaltic Volcanoes: Genetic Classification, Growth, Geomorphology and Degradation. *Updates in Volcanology - New Advances in Understanding Volcanic Systems*, 3–88.

Kervyn, M., Ernst, G. G. J., Carracedo, J.-C., & Jacobs, P. (2012). Geomorphometric variability of "monogenetic" volcanic cones: evidence from Mauna Kea, Lanzarote and experimental cones. *Geomorphology*, *136*(1), 59–75. doi: 10.1016/j.geomorph.2011.04.009

Malin, M. C., Bell, J. F., Cantor, B. A., Caplinger, M. A., Calvin, W. M., Clancy, R. T., ... Wolff, M. J. (2007). Context Camera Investigation on board the Mars Reconnaissance Orbiter. *Journal of Geophysical Research*, *112*(E5), E05S04. doi: 10.1029/2006JE002808

Manfredi, L. (2012). *Volcanic History of the Tempe Volcanic Province* (Unpublished master's thesis). Arizona State University.

Mège, D., & Masson, P. (1996). Stress models for Tharsis formation, Mars. *Planetary and Space Science*, *44*(12), 1471–1497. doi: 10.1016/S0032-0633(96)00112-2

Michalski, J. R., & Bleacher, J. E. (2013). Supervolcanoes within an ancient volcanic province in Arabia Terra, Mars. *Nature*, *502*(7469), 47–52. doi: 10.1038/nature12482

Mitchell, K. L. (2005). Coupled conduit flow and shape in explosive volcanic eruptions. *Journal of volcanology and geothermal research*, *143*(1-3), 187–203.

Montési, L. G. (2001). Concentric dikes on the flanks of pavonis mons: Implications for the evolution of martian shield volcanoes and mantle plumes. *Mantle Plumes: Their Identification Through Time*, *352*, 165.

Montési, L. G., Behn, M. D., Hebert, L. B., Lin, J., & Barry, J. L. (2011). Controls on melt migration and extraction at the ultraslow Southwest Indian Ridge 10–16 E. *Journal of Geophysical Research: Solid Earth*, *116*(B10).

Moore, J. G., & Clague, D. A. (1992). Volcano growth and evolution of the island of Hawaii. *Geological Society of America Bulletin*, *104*(11), 1471–1484. doi: 10.1130/0016-7606(1992)104<1471:VGAEOT>2.3.CO;2

Mouginis-Mark, P. (2018). *Olympus Mons volcano, Mars: A photogeologic view and new insights.* doi: 10.1016/j.chemer.2017.11.006

Mouginis-Mark, P. J., & Wilson, L. (2019). Late-stage intrusive activity at Olympus

Mons, Mars: Summit inflation and giant dike formation. *Icarus*. doi: 10.1016/j.icarus.2018.09.038

Mouginis-Mark, P. J., Wilson, L., & Zuber, M. T. (1992). The physical volcanology of Mars. In H. H. Kieffer, et al. (Ed.), *Mars* (pp. 424–452). Tucson: The University of Arizona Press.

Neesemann, A., van Gasselt, S., Hauber, E., & Neukum, G. (2010). Detailed mapping of Tempe Terra, Mars: Geology, tectonic and stratigraphy of refined units. In *EGU General Assembly Conference Abstracts* (Vol. 12, p. 6837).

Neukum, G., Jaumann, R., Hoffmann, H., Hauber, E., Head, J. W., Basilevsky, A. T., ... The HRSC Co-Investigator Team (2004). Recent and episodic volcanic and glacial activity on Mars revealed by the High Resolution Stereo Camera. *Nature*, *432*(7020), 971–979. doi: 10.1038/nature03231

Parcheta, C., Fagents, S., Swanson, D. A., Houghton, B. F., & Ericksen, T. (2015). Hawaiian fissure fountains: Quantifying vent and shallow conduit geometry, episode 1 of the 1969–1974 Mauna Ulu eruption. In R. Carey, V. Cayol, M. Poland, & D. Weis (Eds.), *Geophysical monograph series.* American Geophysical Union. doi: 10.1002/9781118872079.ch17

Peters, S. I., & Christensen, P. R. (2017). Flank vents and graben as indicators of Late Amazonian volcanotectonic activity on Olympus Mons. *Journal of Geophysical Research: Planets*. doi: 10.1002/2016JE005108

Plescia, J. B. (1981). The tempe volcanic province of mars and comparisons with the snake river plains of idaho. *Icarus*, *45*(3), 586–601.

Porter, S. C. (1972). Distribution, Morphology, and Size Frequency of Cinder Cones on Mauna Kea Volcano, Hawaii. *GSA Bulletin*, *83*(12), 3607–3612. doi: 10.1130/0016-7606(1972)83[3607:dmasfo]2.0.co;2

Reynolds, H. I., Gudmundsson, M. T., Högnadóttir, T., Magnússon, E., & Pálsson, F. (2017). Subglacial volcanic activity above a lateral dyke path during the 2014–2015 Bárdarbunga-Holuhraun rifting episode, Iceland. *Bulletin of Volcanology*, *79*(6), 38. doi: 10.1007/s00445-017-1122-z

Richardson, J. A., Bleacher, J. E., & Baptista, A. A. R. (2010). Identification of Volcanic Ridge in Northern Syria Planum, Mars: Constraint on Geologic History of Syria. In *Lunar and Planetary Science Conference, abs. 1427* (Vol. 41, p. 1427).

Richardson, J. A., Bleacher, J. E., Connor, C. B., & Glaze, L. S. (2018). Trends in Distributed Volcanism Across Tharsis Province, Mars. In *Lunar and Planetary Science Conference, abs. 2045* (Vol. 49).

Richardson, J. A., Bleacher, J. E., Connor, C. B., & Glaze, L. S. (2020). *Tharsis volcanic vents enhanced database.* Zenodo. doi: 10.5281/zenodo.4275144

Richardson, J. A., Bleacher, J. E., & Glaze, L. S. (2013). The volcanic history of Syria Planum, Mars. *Journal of Volcanology and Geothermal Research*, *252*, 1–13. doi: 10.1016/j.jvolgeores.2012.11.007

Richardson, J. A., Wilson, J. A., Connor, C. B., Bleacher, J. E., & Kiyosugi, K. (2017). Recurrence rate and magma effusion rate for the latest volcanism on Arsia Mons, Mars. *Earth and Planetary Science Letters*, *458*, 170–178. doi: 10.1016/j.epsl.2016.10.040

Rowland, S. K. (1996). Slopes, lava flow volumes, and vent distributions on volcan fernandina, galapagos islands. *Journal of Geophysical Research: Solid Earth*, *101*(B12), 27657–27672.

Rowland, S. K., & Walker, G. P. L. (1990). Pahoehoe and aa in Hawaii: volumetric flow rate controls the lava structure. *Bulletin of Volcanology*, *52*, 615–628. doi: 10.1007/BF00301212

Scanlon, K. E., Head, J. W., & Marchant, D. R. (2015). Remnant buried ice in the equatorial regions of Mars: Morphological indicators associated with the Arsia Mons tropical mountain glacier deposits. *Planetary and Space Science*, *111*, 144–154. doi: 10.1016/j.pss.2015.03.024

Settle, M. (1979). Structure and Emplacement of Cinder Cone Fields. *American Journal of Science*, *279*(10), 1089–1107. doi: 10.2475/ajs.279.10.1089

Smith, D., Neumann, G., Arvidson, R., Guinness, E., & Slavney, S. (2003). Mars global surveyor laser altimeter mission experiment gridded data record (mgs-m-mola-5-megdr-l3-v1. 0). *National Aeronautics and Space Administration Planetary Data System.*

Smith, D. E., & Zuber, M. T. (1996). The shape of mars and the topographic signature of the hemispheric dichotomy. *Science*. doi: 10.1126/science.271.5246.184

Som, S. M., Greenberg, H. M., & Montgomery, D. R. (2008). The Mars Orbiter Laser Altimeter dataset: Limitations and improvements. *The Mars Journal*. doi: 10.1555/mars.2008.0002

Sori, M. M., & Bramson, A. M. (2019). Water on Mars, With a Grain of Salt: Local Heat Anomalies Are Required for Basal Melting of Ice at the South Pole Today. *Geophysical Research Letters*, *46*(3), 1222–1231. doi: 10.1029/2018GL080985

Spudis, P. D., McGovern, P. J., & Kiefer, W. S. (2013). Large shield volcanoes on the moon. *Journal of Geophysical Research: Planets*, *118*(5), 1063–1081.

Tadini, A., Bonali, F., Corazzato, C., Cortés, J., Tibaldi, A., & Valentine, G. (2014). Spatial distribution and structural analysis of vents in the Lunar Crater Volcanic Field (Nevada, USA). *Bulletin of Volcanology*, *76*(11), 877.

Tanaka, K. L., & Davis, P. A. (1988). Tectonic history of the Syria Planum province of Mars. *Journal of Geophysical Research: Solid Earth*, *93*(B12), 14893–14917. doi: 10.1029/JB093iB12p14893

Tanaka, K. L., Skinner, J. A., Dohm, J. M., Irwin, R. P., Kolb, E. J., Fortezzo, C. M., ... Hare, T. M. (2014). Geologic Map of Mars. *U.S. Geological Survey Geologic Investigations*, 3292. doi: 10.3133/sim3292

Valentine, G., & Gregg, T. (2008). Continental basaltic volcanoes—processes and problems. *Journal of Volcanology and Geothermal Research*, *177*(4), 857–873.

Valentine, G. A., & Connor, C. B. (2015). Basaltic volcanic fields. In *The encyclopedia of volcanoes* (pp. 423–439). Elsevier.

Wadge, G., & Cross, A. (1988). Quantitative methods for detecting aligned points: An application to the volcanic vents of the Michoacan-Guanajuato volcanic field, Mexico. *Geology*, *16*(9), 815–818. doi: 10.1130/0091-7613(1988)016<0815:QMFDAP>2.3.CO;2

Wadge, G., & Cross, A. M. (1989). Identification and analysis of the alignments of point-like features in remotely-sensed imagery. Volcanic cones in the Pinacate Volcanic Field, Mexico. *International Journal of Remote Sensing*, *10*, 455–474. doi: 10.1080/01431168908903885

Werner, S. C. (2009). The global martian volcanic evolutionary history. *Icarus*, *201*(1), 44–68. doi: 10.1016/j.icarus.2008.12.019

Williams, D. A., Greeley, R., Fergason, R. L., Kuzmin, R., McCord, T. B., Combe, J. P., ... Neukum, G. (2009). The Circum-Hellas Volcanic Province, Mars: Overview. *Planetary and Space Science*, *57*(8-9), 895–916. doi: 10.1016/j.pss.2008.08.010

Witt, T., Walter, T. R., Müller, D., Guðmundsson, M. T., & Schöpa, A. (2018, dec). The Relationship Between Lava Fountaining and Vent Morphology for the 2014–2015 Holuhraun Eruption, Iceland, Analyzed by Video Monitoring and Topographic Mapping. *Frontiers in Earth Science*, *6*, 235. doi: 10.3389/feart.2018.00235